

Tropospheric Ozone: The Role of Transport

H. LEVY II, J. D. MAHLMAN, AND W. J. MOXIM

Geophysical Fluid Dynamics Laboratory, NOAA, Princeton University, New Jersey

S. C. LIU

Aeronomy Laboratory, NOAA, Boulder, Colorado

The Geophysical Fluid Dynamics Laboratory general circulation/transport model, with photochemistry in the top level (middle stratosphere) only, is used to simulate global tropospheric ozone distributions for upper and lower limits of surface removal rates. We compared these simulations with available observations and find that large-scale atmospheric transport plays a major role in the behavior of tropospheric ozone. Furthermore, we identify potential roles for tropospheric chemistry, discover defects in the model's simulations of transport, and gain a more global picture of tropospheric ozone. The transport model's mean cross-tropopause flux is in the range of previous estimates, and the shapes of the simulated vertical profiles of mixing ratio and percent standard deviation are in good agreement with observations. South of 40°N, the simulated and observed latitude gradients are the same, the upper and lower limit calculations bracket measured values, and the seasonal cycles are well reproduced. While the transport model simulates a wide range of tropospheric ozone climatology, there are a significant number of disagreements. The need for additional ozone destruction in the maritime boundary layer suggests a role for chemical destruction, while in the continental boundary layer, it appears that chemical production, a seasonal cycle in surface deposition, and improved boundary layer transport are all required. The two major defects in the simulated "free troposphere" are (1) excess ozone at high latitudes of the northern hemisphere (NH) and (2) spring rather than summer maxima and fall rather than winter minima at NH mid- and high latitudes. While defect 1 has a number of possible causes, deficiencies in model transport play a major role. Although similar transport defects have not been ruled out for defect 2, tropospheric chemistry appears to be needed. Separate calculations of the net chemical production and loss demonstrate that this is a complex problem. The most likely solution involves the transport control of NO_x which controls the ozone chemistry.

1. INTRODUCTION

Ozone is an important oxidant in its own right, a precursor for highly reactive radicals, and a significant absorber of ultraviolet and infrared radiation. It is therefore important that we understand the behavior of ozone in the troposphere and are able to predict its response to perturbations, both natural and anthropogenic.

Rather than the issue of global or column budgets which are currently beyond realistic calculation or verification by observations, we focus on climatology (mean values, spatial variability, and time variability). We explore the role of atmospheric transport by comparing available observations with the results of a Geophysical Fluid Dynamics Laboratory (GFDL) general circulation/transport model which specifically excludes tropospheric chemistry. This model has ozone chemistry in the top layer (middle stratosphere) only and simulates global ozone distributions for upper and lower limits of surface removal rates. Disagreements between observations and the simulations serve to identify potential roles for tropospheric chemistry, though defects in the model transport, the surface removal formulation, and the observational data must also be considered. By combining the global, though far from perfect, simulated ozone fields with the accurate, though greatly limited, observational data, we gain a more complete picture of ozone in the troposphere. A number of smaller-scale transport processes (e.g., boundary layer turbulence, diurnal fluctuations, moist convection) are not resolved explicitly by the model. While we attempt to capture their effects implicitly

through parameterizations which key off the large-scale forcing, transport in the model's continental boundary layer is poorly simulated.

Two recent reviews [Bojkov, 1984; Fishman, 1984] present a detailed history of the debate over chemical versus transport control of tropospheric ozone. They conclude that both chemistry and transport play an important role and that the actual combination of chemical and physical processes controlling ozone are not clearly understood. A brief summary of the last 10 years debate is presented here.

The earliest view of tropospheric ozone assumed stratospheric injection and surface destruction with no intervening chemistry [e.g., Junge, 1962]. There exists a considerable body of observations which support this position: the Fabian and Pruchniewicz [1977] measurements of the meridional distribution of tropospheric ozone from both surface stations and aircraft flights; the Husain *et al.* [1977] and Husain and Dutkiewicz [1979] calculations, based on measurements of ⁷Be/O₃ ratios in the stratosphere and ⁷Be concentrations at the ground, that show at least half of the tropospheric ozone being transported from the stratosphere; the Singh *et al.* [1978] O₃ time series from remote surface stations and aircraft ozone measurements that are best explained by transport; and the Chatfield and Harrison [1977] analysis of Hering and Borden [1967] ozonesonde data which finds an increased injection across the tropopause in the spring followed by southward transport with an ozone lifetime of months. Furthermore, the stratospheric injection of ozone has been observed directly [Danielsen, 1968; Danielsen and Mohn, 1977], inferred from radioactivity measurements [Husain *et al.*, 1977; Dutkiewicz and Husain, 1979], and calculated from general circulation/transport models [Mahlman *et al.*, 1980, hereafter MLM80; Gidel and Shapiro, 1980]. These different approaches

This paper is not subject to U.S. copyright. Published in 1985 by the American Geophysical Union.

Paper number 4D1447.

all arrive at a cross-tropopause flux in the range of $3\text{--}12 \times 10^{10}$ molecules $\text{cm}^{-2} \text{s}^{-1}$. The surface destruction of ozone has been observed directly [Aldaz, 1969; Galbally and Roy, 1980] and inferred from flux measurements in the boundary layer [Lenschow et al., 1980, 1982; Wesely et al., 1981; Pearson and Stedman, 1980]. Estimates of surface deposition flux [Fabian and Junge, 1970; Galbally and Roy, 1980; Fishman et al., 1979; Fishman, 1984] are in the same range as stratospheric injection.

Following the prediction of a vigorous radical chemistry in the troposphere [Levy, 1971], Crutzen [1973, 1974] calculated column rates of chemical production and destruction which equaled or exceeded the estimated transport fluxes, and Chameides and Walker [1973] argued that tropospheric ozone was in or close to chemical steady state. While there have been significant changes in rate coefficients, reaction mechanisms, and accepted trace species concentrations, later calculations confirm the large rates of chemical production and destruction [Fishman and Crutzen, 1977, 1978; Liu, 1977; Stewart et al., 1977]. Such calculations are strongly dependent on the global distribution of NO_x , which is highly variable and not well known. However, the chemical production of O_3 in the polluted boundary layer is well known. Furthermore, Fishman and Seiler [1983] argue that positive correlations between the fluctuations in simultaneous vertical profiles of O_3 and CO imply a boundary layer source for both trace gases.

Recently, a combination of the classical transport theory and the chemical theory was proposed by Liu et al. [1980]. Ozone chemical production is expected to occur mainly in the upper troposphere with the precursor NO_x being transported down from the stratosphere [Levy et al., 1980] or produced by cloud to cloud lightning [Liu et al., 1983]. In the lower troposphere the net result of atmospheric chemistry should be ozone destruction. This theory depends critically on a tropospheric NO_x distribution which has its maximum values in the upper troposphere and minimum values at the surface. An analysis of recent measurements of NO_x in the unpolluted atmosphere [Kley et al., 1981] finds just such a distribution, and Liu et al. [1983] find that chemical destruction is needed to explain the low levels of O_3 (5–10 ppbv) observed in the tropical marine boundary layer. However, at this time the lack of joint NO_x and O_3 measurements precludes any general conclusions about the role of O_3 chemistry on a global scale.

2. MODEL DESCRIPTION

2.1. Transport

These numerical experiments employed the GFDL general circulation/transport model. This model has already been used to study the global dispersion and rainout of radioactive debris from an idealized nuclear weapons test [Mahlman and Moxim, 1978, hereafter MM78], the three-dimensional structure and behavior of a simplified ozone tracer (MLM80) and the tropospheric behavior of N_2O [Levy et al., 1982, hereafter LMM82]. This model has 11 terrain following (σ) levels in the vertical with standard heights of 31.4, 22.3, 18.8, 15.5, 12.0, 8.7, 5.5, 3.1, 1.5, 0.5, and 0.08 km and a horizontal grid size of approximately 265 km. The continuity equation for the volume mixing ratio of any trace gas R , in σ coordinates, is given by

$$\frac{\partial R p_*}{\partial t} = -\nabla_{\sigma} \cdot V_2 p_* R - \frac{\partial}{\partial \sigma} \sigma p_* R + \text{FILLING} \\ + \text{DIFFUSION} + p p_* - L p_* R - D p_* R \quad (1)$$

where p_* is surface pressure at a given grid point, V_2 is the horizontal wind vector, σ is the vertical motion in σ coordinates, $P - LR$ is the sum of chemical production and loss of R , and D is the surface destruction rate coefficient (s^{-1}) of R . The advection terms are evaluated with centered time differencing, fourth-order centered space differencing in the vertical and second order in the horizontal. A simple forward Euler step is used for DIFFUSION and the chemical terms (see MM78 for details). DIFFUSION (parameterized subgrid-scale vertical and horizontal diffusion) is discussed in the study of tropospheric N_2O (LMM82). FILLING, a computational adjustment of negative mixing ratios which is mass conservative but diffusive in nature, is described in MM78. The wind fields used in (1) are the 6-hour time-averaged wind fields generated by a GFDL general circulation model [Manabe et al., 1974] for 1 year. This general circulation model (GCM) has no diurnal variation of insolation and thus will not realistically simulate atmospheric fluctuations with periods shorter than 1 day. The preparation of the input data, the relevant features of the general circulation model providing it, and the numerical techniques used to integrate (1) have all been described previously (MM78 and LMM82).

2.2. Source

The model's source of tropospheric ozone is the net chemical production of ozone in its top level. There is no chemistry in any of the lower levels. This middle stratosphere ozone is transported downward across the tropopause and ultimately removed at the surface. These mixing ratios are calculated with a daily averaged simplified chemistry which varies with longitude, latitude, and season. Nitrogen and water chemistries are included, but chlorine chemistry is not. H_2O is prescribed with a constant mixing ratio of 3 ppmv. The mixing ratio of NO_y ($\text{NO} + \text{NO}_2 + \text{HNO}_3$) is set at 17.5 ppbv for all latitudes to force the correct equatorial 10 mbar O_3 . While this parameterization is not appropriate for a sensitivity study, it is sufficient to simulate the observed latitude gradient, seasonal cycle, and absolute values of O_3 at 10 mbar (MLM80). The chemical model has been described in some detail in an earlier paper. (See section 2.6.2 of MLM80. $P - LR$ in (1) is the same as SOURCE-SINKS in equations 2.2–2.10 of MLM80.) The seasonal and latitudinal behavior of the model's total ozone (spring maxima at high latitudes of both hemispheres and a minimum throughout the year in the tropics) are in qualitative agreement with observation, though the model exaggerates the hemispheric asymmetry. The result is a stratospheric ozone field with the correct latitudinal and seasonal variability. The total ozone from a similar experiment where tropospheric destruction involved rainout as well as surface removal is compared with observation in Figures 4.2 and 4.3 of MLM80.

In these simulations, the cross-tropopause flux of ozone is 5×10^{10} molecules $\text{cm}^{-2} \text{s}^{-1}$, in harmony with past estimates and with an earlier study (MLM80). As has been demonstrated previously (MLM80), the model's transport across the tropopause is determined by the mixing ratio gradient in the model's stratosphere. This stratospheric gradient is controlled by the model's resolved motions but is also affected by the lack of photochemistry in the model's lower stratosphere. At this time we do not know whether the addition of lower stratospheric photochemistry would increase or decrease the global cross-tropopause flux. We do expect that such an added photochemistry would decrease the hemispheric asymmetry in the flux.

2.3. Destruction

In most cases the surface mixing ratio will be less than the bulk boundary layer value, only approaching it in the case of very strong mixing and/or small values of deposition velocity (W_0). This point has already been addressed by *Fabian and Junge* [1970] and *Galbally and Roy* [1980], who have proposed methods for calculating R at the surface ($R_{11.5}$) from R at some height in the boundary layer. We assume that the bottom half of the lowest level is in steady state, with surface deposition just balanced by the turbulent flux. The surface destruction rate coefficient in (1) is then given by

$$D = \frac{W_0}{\Delta z} \frac{1}{1 + (W_0/C_D)|V_{\text{eff}}|} \quad (2)$$

where W_0 is the deposition velocity (in centimeters per second), Δz is the thickness of the bottom half level (in centimeters) with a standard value of 8×10^3 cm, C_D is a globally averaged surface drag coefficient (0.002), and $|V_{\text{eff}}|$ is the effective surface wind speed. Both Δz and $|V_{\text{eff}}|$ are calculated by the model with no diurnal dependence and $1 + W_0/C_D |V_{\text{eff}}|$ is the effective reduction of R_{11} , the model mixing ratio in the bottom level.

W_0 for ozone is highly variable depending not only on the nature of the surface but also, in the case of vegetation, on plant type and season. There have been direct box measurements over a number of surfaces [*Aldaz*, 1969; *Galbally and Roy*, 1980] and indirect measurements using eddy correlation techniques [*Pearson and Stedman*, 1980; *Lenschow et al.*, 1980, 1982; *Wesely et al.*, 1981]. The indirect method calculates the eddy flux of a gas, in this case O_3 , at a given height in the boundary layer and equates it to the surface deposition flux. From this an effective W_0 is calculated relative to the mixing ratio at the height of the measurement not at the surface. Ozone surface removal does appear to break down into two main categories: (1) land either bare or covered with vegetation, where W_0 ranges from 2.0 cm s^{-1} over daytime forests and cultivated crops to 0.2 cm s^{-1} over nighttime grassland and (2) oceans and snow where measurements range from 0.10 to 0.02 cm s^{-1} .

Given the wide range of measured values and the wide range of available surface types and vegetation types, we do not believe that a realistic and detailed simulation of surface loss is possible on a global scale at this time. Rather we choose to take advantage of the approximate factor of 10 difference between W_0 for land with or without vegetation and for ocean and snow. A parameterization of seasonal variability of W_0 over land is not included in this study. The "fast destruction" experiment uses $W_0 = 1.0 \text{ cm s}^{-1}$ over land and 0.1 cm s^{-1} over ice and ocean. The "slow destruction" experiment has $W_0 = 0.2 \text{ cm s}^{-1}$ over land and 0.02 cm s^{-1} over ice and ocean. All land north of 72°N and south of 72°S is assumed to be ice covered. Upper and lower limits of W_0 are used in the calculations to bracket the mean values and the level of variability, both spatial and temporal, in transport-controlled tropospheric ozone.

The large-scale features of the tropospheric ozone distribution (hemispheric and latitude gradients, mean vertical profiles, seasonal variations in local monthly mean values) should be relatively insensitive to small-scale variations in deposition velocity and should be dominated by the land-sea contrast. The simulated seasonal variations over land may be sensitive to the lack of seasonal variability in W_0 . By using an idealized and highly simplified distribution of deposition velocity we

may not be able to simulate realistically the specific local ozone behavior, particularly in the boundary layer over a non-uniform surface. The general circulation model's simulation of boundary layer dynamics is itself quite crude and, in particular, has no diurnal variation. Therefore we do not expect the transport model to simulate surface ozone time series accurately over most land, even if photochemistry is included.

3. MODEL RESULTS

In this section we will first examine the zonally averaged global fields generated by the model. Even though observed fields are not available for full comparison with the model simulations, we can learn much about the full three-dimensional variability of tropospheric ozone from a model which has already been shown to simulate a qualitatively correct atmospheric transport.

3.1. Global Fields

Latitude-longitude plots of monthly mean ozone mixing ratios ($\bar{R}_{O_3}^{\text{mm}}$) in the surface layer and on 500- and 190-mbar surfaces are given for January and July in Figure 1. Since the structural features are the same in both the "slow destruction" and "fast destruction" integrations, we only show the results from one, in this case "slow destruction," when detailed comparisons with observation are not possible. The contours have been stopped at 72°N and 72°S because of geographical distortion. There is no particularly interesting information above 72° , as can be seen from the latitude-height plots in Figure 2. Those high-latitude features of interest are already apparent by 60° .

In the surface level the land-sea contrast in W_0 dominates with deep minima in $\bar{R}_{O_3}^{\text{mm}}$ forming over the continental interiors during each hemisphere's winter. The minima found for the "fast destruction" case are much too low and not in agreement with observations. Even summertime convection does not completely remove the minima. The deep wintertime minima and exaggerated vertical gradients in the continental boundary layer will be discussed in section 4.2.1. Other major features of the January surface field, maxima over the northern Pacific and Atlantic, are the result of strong downward transport and relatively low W_0 .

The 500-mbar fields in Figure 1 are representative of the "free troposphere," that region lying above the boundary layer and below the tropopause region. These fields show little longitudinal structure south of 30°N and a very weak latitude gradient in the southern hemisphere. In the northern hemisphere there is a much stronger latitude gradient which weakens somewhat in July. A weak local maximum forms around 50°N over the North Pacific in the winter as a result of the systematic downward transport from the stratosphere in association with the strong jet stream off the east coast of Asia (Japan jet). This cross-tropopause transport feature exists in both the real atmosphere and the model and has been previously discussed in considerable detail [*Manabe and Mahlman*, 1976; *MM78*; and *MLM80*].

Chatfield and Harrison [1977] found an east-west gradient in annual mean ozone in the middle troposphere over North America when they analyzed the data from *Hering and Borden* [1967]. While a similar gradient is observed in the upper United States during the model's winter simulation (see the January 500-mbar panel in Figure 1), it is not at as low a latitude as the observations. Furthermore, the model gradient does not persist throughout the year nor does the model pro-

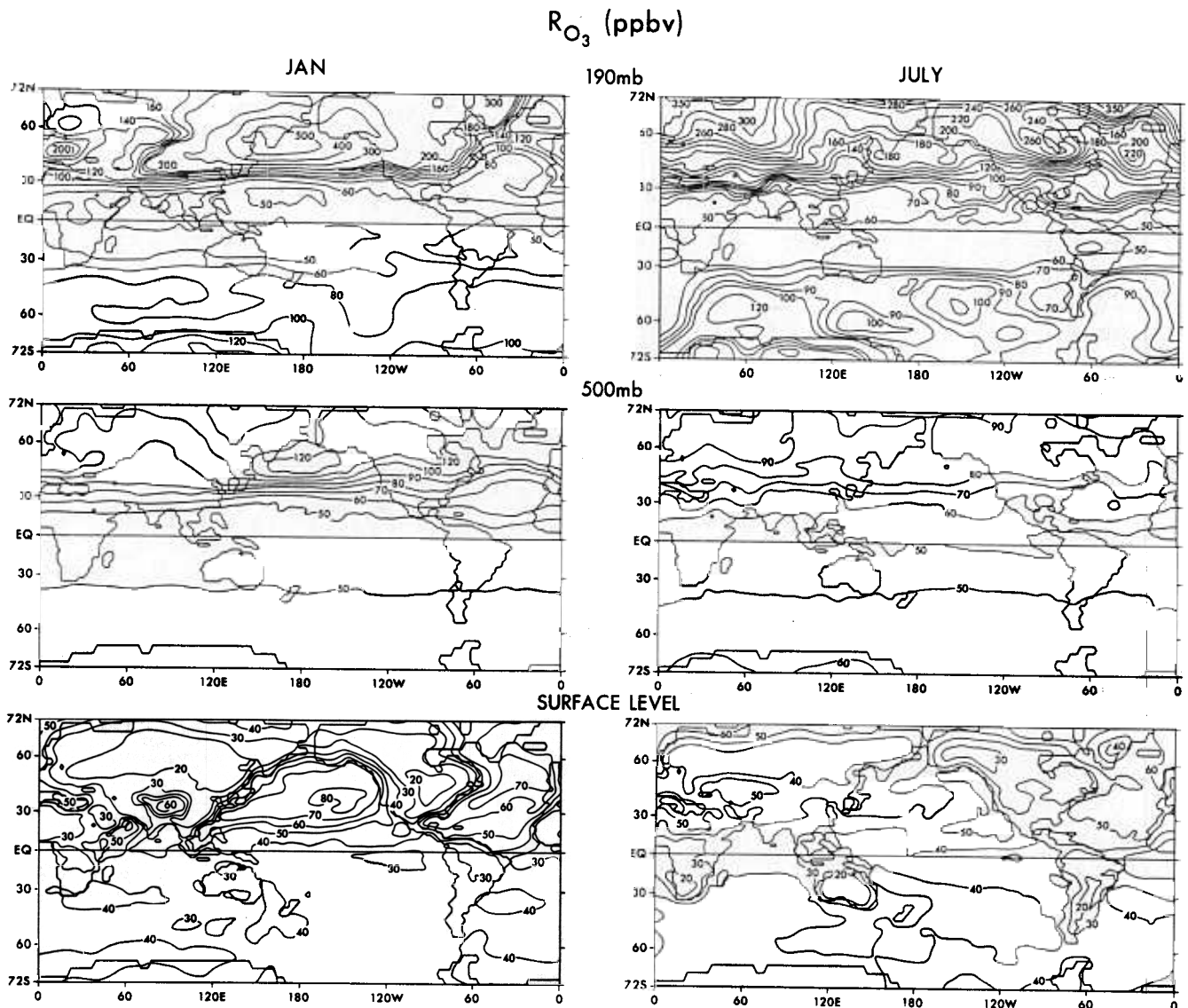


Fig. 1. Local monthly mean ozone mixing ratios from the "slow destruction" simulation are presented for three representative tropospheric levels (surface level, 500 mbar, 190 mbar) for January and July.

duce the relatively high values observed by *Hering and Borden* [1967] over Florida.

The $\bar{R}_{O_3}^{mn}$ fields at 190 mbar reveal clearly the major cause of the model's interhemispheric asymmetry in tropospheric ozone. The winter maximum in the northern hemisphere is localized in the region of the tropospheric Aleutian low and reaches 500 ppbv. Even in summer, $\bar{R}_{O_3}^{mn}$ at 190 mbar exceeds 200 ppbv at high latitudes. In contrast, the winter maximum in the southern hemisphere is much more zonal and barely exceeds 100 ppbv. In the winter, northern hemisphere cross-tropopause transport is very strong and dominated by downward advection on the north side of the Japan jet. In the southern hemisphere (SH) troposphere there is no similar strong stationary process, and poleward downward transport is much weaker in the SH stratosphere. This has already been discussed in great detail in an earlier paper on stratospheric ozone (MLM80). The net result is that the model's cross-tropopause flux in the northern hemisphere is about twice that in the southern hemisphere. While there is observational evidence to support the existence of a hemispheric asymmetry in

the real cross-tropopause flux, it is quite probable that the model exaggerates the difference (MLM80).

3.2. Zonal Average Fields

Latitude-height plots of the zonal monthly mean ozone mixing ratio ($\bar{R}_{O_3}^{\lambda}$) are given in Figure 2 for representative months from each of the four seasons. Since the zonal mean structure is the same for both simulations, we again show model results only from the "slow destruction" integration. Outside of the boundary layer, $\bar{R}_{O_3}^{\lambda}$ in the northern hemisphere exceeds those values in the southern hemisphere, particularly at high latitudes. While this northern hemisphere excess holds throughout the year, it is lowest in October when the two hemispheres are almost in balance between 40°N and 40°S. This seasonal behavior in the "free troposphere" is qualitatively consistent with the observations of *Fabian and Pruchniewicz* [1977] and the comparison between data from Boulder, Colorado, and Aspendale, Australia, made by *Pittock* [1977]. In the tropics and the southern hemisphere subtropics the $\bar{R}_{O_3}^{\lambda}$ field has very weak horizontal and vertical gradients

CLASSICAL OZONE "SLOW DESTRUCTION"

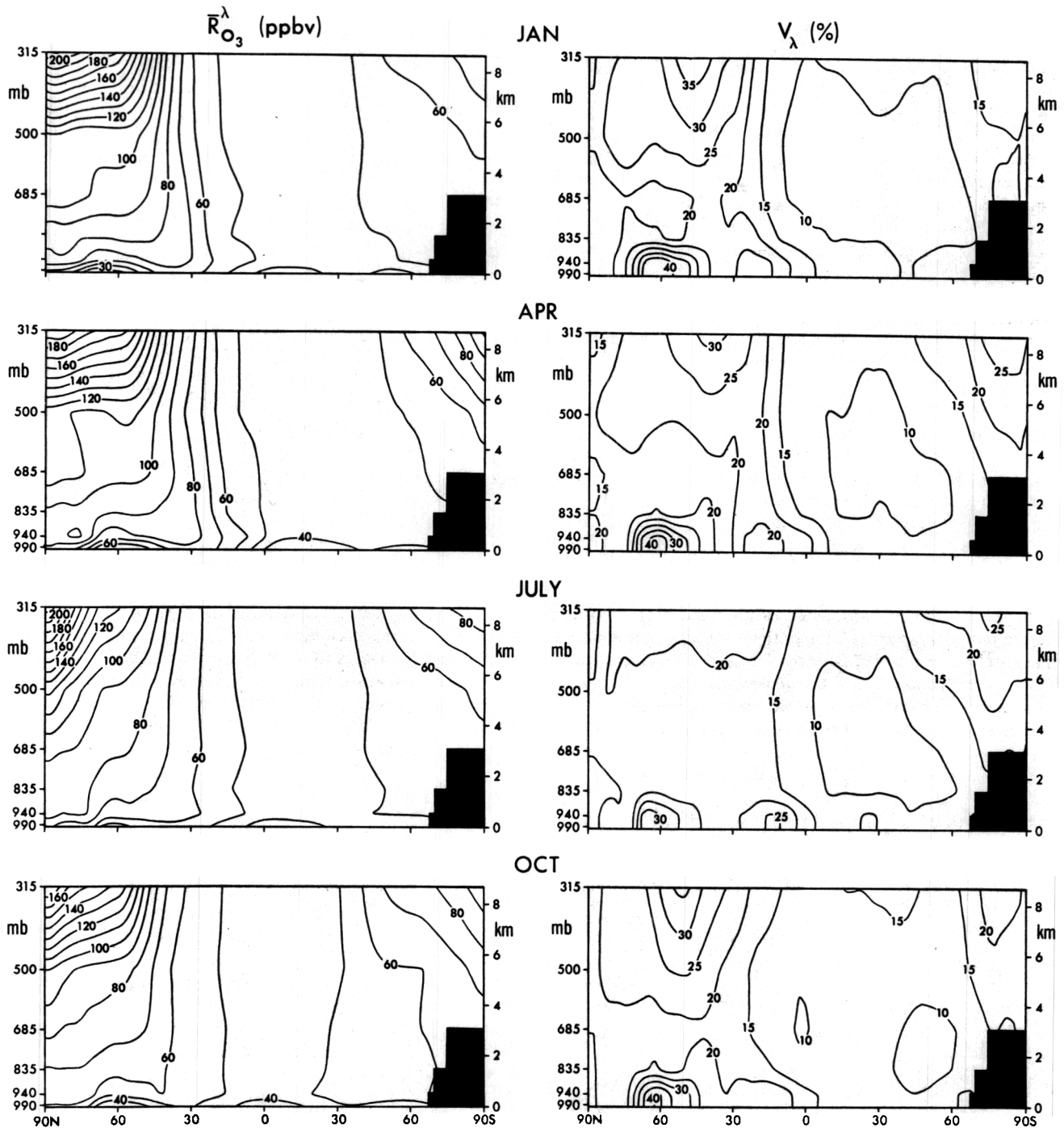


Fig. 2. Latitude-altitude plots of the zonally averaged monthly means as well as the percent standard deviations relative to the zonal means are presented from the "slow destruction" simulation of tropospheric ozone.

throughout the "free troposphere" because of an ocean-dominated weak deposition velocity, a weak cross-tropopause flux, and a relatively strong vertical mixing.

The monthly averaged percent standard deviation of local mixing ratios relative to the zonal mean V_λ is also plotted in Figure 2 as a function of latitude and height for the "slow destruction" experiment. V_λ , which is calculated around a given latitude circle, provides a measure of the monthly averaged spatial variability of local values and is strongly in-

fluenced by stationary eddy processes. In general, V_λ is small throughout the tropics and southern hemisphere subtropics. It reaches a maximum in the upper troposphere high latitudes of both hemispheres. These larger values spread throughout most of the mid-latitude troposphere of each hemisphere during their respective winter and spring. The large spatial variability of ozone in the mid-latitude boundary layer of the northern hemisphere is, in large part, a result of the land-sea contrast in deposition velocity.

4. COMPARISON OF SIMULATIONS AND OBSERVATIONS

An acceptable data base of tropospheric ozone measurements is urgently needed, not only for this paper but also for the field of tropospheric chemistry as a whole. Existing satellite and Umkehr data are not easily used in the troposphere. While Dütsch [1974] has constructed a global field of tropospheric ozone for the four seasons from available data, he observed that the current network of ozonesonde stations is not adequate, even if one ignores the problems arising from the use of different sensors and operational procedures as well as serious questions about absolute accuracy. Almost all of the stations are in the northern hemisphere and most of those at mid-latitude over land. There are a few operating at high latitude, one in the tropics, and one at mid-latitude in the southern hemisphere. Even when all previous stations are included, there is minimal improvement in the global coverage. At this time there are no ozonesonde data over any of the oceans.

A few single north-south transects through the middle troposphere with relatively accurate ozone sensors are available [Routhier et al., 1980; Seiler and Fishman, 1981; Gregory et al., 1984]. The one data set that provides more than a north-south snapshot has severe problems with absolute calibration of the sensor [Fabian and Pruchniewicz, 1977]. The multiyear continuous surface measurements of Oltmans [1981] and I. E. Galbally (private communication, 1984) appear to be the best data in terms of absolute accuracy, length, and completeness of record, and care of analysis, but they are limited to the boundary layer. Although there is some question about the absolute accuracy of Brewer-Mast and electrochemical cell (ECC) ozonesonde data [Attmannspacher and Dütsch, 1981], the relative vertical and seasonal structure should be valid. Furthermore the vertical profile time series will reveal local, regional, and global properties of tropospheric ozone. We use the analysis of unpublished Hering and Borden data by Chatfield and Harrison [1977] and the analysis by J. A. Logan (manuscript in preparation, 1984) of the Canadian ozonesonde network, the Japanese ozonesonde network, the Hohenpeissenberg ozonesonde data [Attmannspacher and Hartmanngruber, 1976], the Payerne ozonesonde data [e.g., Dütsch and Ling, 1973] and the Wallops Island, Virginia, data, all of which are compiled in Ozone Data for the World, Atmospheric Environment Service, Canada. The analyses by Pittock [1977] of the Aspendale, Australia, ozonesonde data and by Kirchhoff et al. [1983] of the Natal, Brazil, data are also used.

4.1. Latitude Structure

While there are not sufficient observational data for comparison with the zonally averaged model results in Figure 2, the Brewer-Mast ozonesonde data from a number of stations are compared in Figure 3 with model results from the same locations. Since the numbers of observations at some of the stations are limited, we use yearly mean values, and we eliminate problems resulting from a lack of intercalibration by restricting the data to a single sensor. Model and observation are compared at 500 mbar to avoid most localized effects from both the tropopause region and the boundary layer. The two observational points at 38°N (Brewer-Mast and ECC) from Wallops Island, Virginia, differ by 20% in their yearly mean and are a clear example of systematic differences between sensors. The mid-latitude maximum reported by Wilcox and Belmont [1977] does not appear for yearly mean data when they are restricted to a single sensor. Data from three Japanese

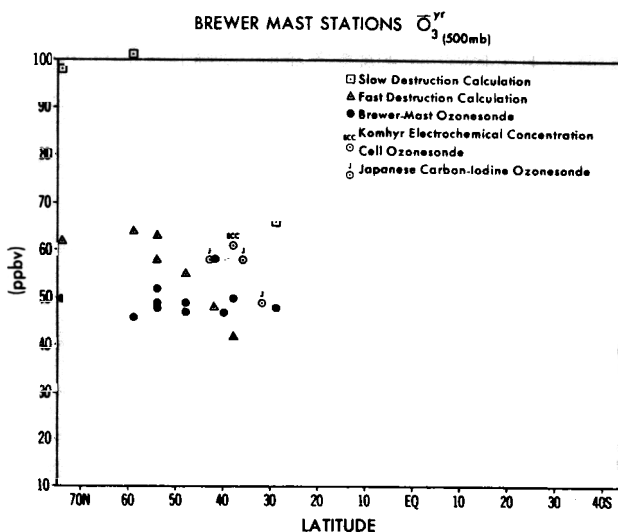


Fig. 3. The 500-mbar yearly averaged Brewer-Mast ozonesonde measurements of ozone from a number of stations are compared with both the "fast destruction" and "slow destruction" model simulations from the same locations. Yearly averages of observations from 500 mbar taken at stations which employ the Komhyr electrochemical concentration cell and the Japanese carbon-iodine cell are included for comparison.

stations which use a third type of sensor are also included in Figure 3.

The Brewer-Mast observational data in Figure 3 are well bracketed by the "fast destruction" and "slow destruction" simulations from 40°S to 40°N. Northward of 40°N the observational data levels off with the single exception of the Bedford, Massachusetts, point (42°N), while the model results keep increasing until 55°N. At that latitude the simulated lower limit of ozone (calculated with the upper limit removal rate) exceeds the observed values by 20%. If the ECC value at 38°N is correct and all the Brewer-Mast data underestimate the true atmospheric value by 20%, the model's high-latitude northern hemisphere model results would look better, but its interhemispheric gradient would not have improved. The three Japanese stations show a different latitude structure, but it is clear from Figure 1 that this is a region of large local gradients which are very sensitive to the mean location of the Japan jet.

In a previous paper on stratospheric ozone (MLM80) we observed that in mid- and high latitudes the simulated ozone fields in the lower stratosphere exceeded observed values and were also above apparent photochemical steady state. We predicted (MLM80) that the inclusion of photochemistry in the lower stratosphere would reduce R_{O_3} in that region, which, in turn, would reduce the net flux into the northern hemisphere (NH) troposphere, and the level of tropospheric O_3 at high latitudes. However, we also find that the mean downward transport is deficient in mid- and high latitudes of the model's stratosphere. This appears to be related to the well-known GCM bias toward excessively cold winter polar temperatures in the lower stratosphere (which, in turn, appear to be caused by insufficient dynamical forcing of the model's stratosphere). A recent comparison of model simulations of N_2O (J. D. Mahlman et al., manuscript in preparation, 1985) with an analysis of N_2O observations (J. Bacmeister et al., manuscript in preparation, 1985) confirms this deficiency in the model's transport which would understate downward flux into the NH troposphere. While the correction of these two model defi-

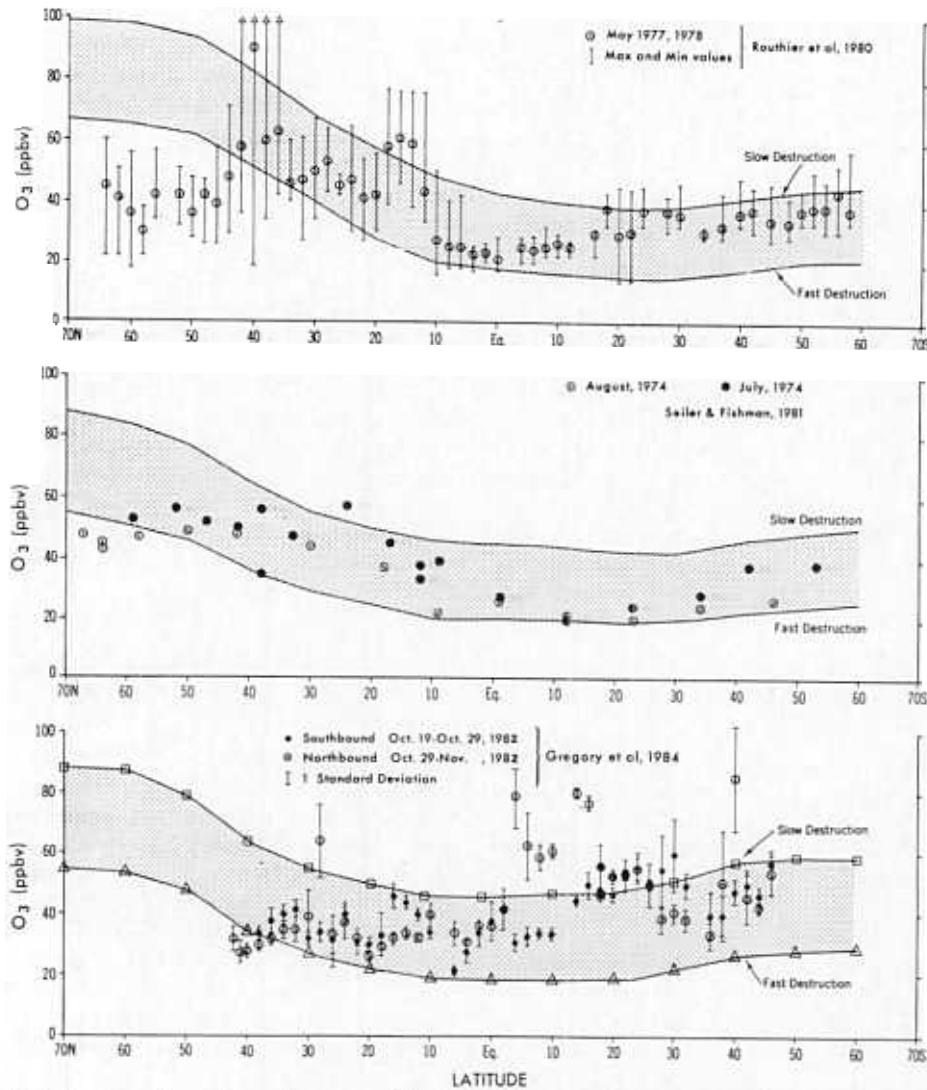


Fig. 4. Instantaneous observations of ozone made in the middle troposphere from aircraft with accurately calibrated ozone measurement devices are compared with the 500-mbar monthly mean zonal averages from both the "fast destruction" and "slow destruction" simulations.

ciencies would tend to cancel, the net result is not obvious. We also suspect that the model's downward fluxes within the troposphere are exaggerated at the pole because of numerical difficulties and that transport out of high latitudes by large-scale disturbances is deficient. A final possibility, tropospheric chemistry, depends on the NO_x distribution at high latitude which is not known. The role of NO_x in O_3 chemistry will be discussed in section 5, and the possibility for chemical destruction of the excess transported O_3 will be explored.

While the Brewer-Mast observations do provide some information on R_{O_3} latitude dependence in the troposphere, the data are very sparse outside of the northern hemisphere mid-latitudes, and there are serious questions about the absolute accuracy of the detector. A series of flights over approximately the same path with an accurate measurement device would provide very useful time average data. Unfortunately, the data of Fabian and Pruchniewicz [1977] do not have an absolute calibration of the measurement device, so only relative latitude profiles are available. Their qualitative results, a NH maximum at mid- and high latitudes which is strongest in winter-spring and weakest in fall, are in good agreement with

the model results of Figure 2. There have been a few flights in the middle troposphere which provide detailed latitude coverage with a sensitive, accurate, and well-calibrated detector: (1) the 1978 GAMETAG flights in the middle troposphere down the western section of North America and out over the Pacific to New Zealand and return [Routhier *et al.*, 1980], (2) a return flight from Cologne to Seattle and down the western coast of the Americas with measurements analyzed for an altitude of 5–6 km [Seiler and Fishman, 1981], and (3) a flight at 5–7 km from Wallops Island, Virginia, to Santiago, Chile, and return to Cheyenne, Wyoming [Gregory *et al.*, 1984]. Unfortunately, these flights only provide a snapshot in time over a band of longitude. At 500 mbar the R_{O_3} fields generated by the transport model show longitudinal variability in the range of 10–20% and temporal variability of 10–25%. This fact and the variability exhibited in the individual data suggest that while a qualitative comparison between the model's time mean zonal data and the measurements from the individual flights is possible, quantitative conclusions are not possible. However, an examination of Figure 4 does identify a number of interesting points.

The data from the May, July, and August flights are well bracketed by the two simulations up to 40°N. Again, at northern hemisphere high latitudes the lower limit model calculation exceeds observation, just as it did for the yearly mean Brewer-Mast data in Figure 3. The extreme values at mid-latitude in the May data of *Routhier et al.* [1980] are thought to be the result of isolated stratospheric intrusions [*Danielsen, 1980*] and would not be expected to show up in the monthly mean model data.

The most unusual results are found in the October data of *Gregory et al.* [1984] where a large southern hemisphere excess is observed in a N-S transect. Equally surprising are the high values (>80 ppmb) observed at 5°S over Peru, even though they are transient and missing on the return leg. The transport model does not simulate either the general southern hemisphere excess observed on both legs of the flight or the large values in the southern hemisphere tropics on the return leg. While our current understanding of tropospheric dynamics and ozone transport can support a transient southern hemisphere excess of O₃ in October and possibly a monthly mean excess, we have difficulty explaining the observed high value of O₃ in the southern hemisphere tropics. Simultaneous NO measurements were uniform and quite low (~15 pptv) throughout the southern hemisphere (A. L. Torres, private communication, 1983) and would appear to rule out any role for chemical production. It should also be noted that *Fabian and Pruchniewicz* [1977] found a similar unexplained peak in the southern hemisphere tropics over Africa during one of their October flights. Information on the spatial scale of the high values as well as the specific meteorological processes is needed.

4.2. Local Observations

There are a number of ozonesonde and surface monitoring stations with multiyear records, relatively accurate absolute calibrations, and consistent and well-founded operational procedures. While the coverage is not sufficient to provide global ozone fields, it is sufficient to challenge a global transport model of tropospheric ozone. The observations are compared with both the "fast destruction" and "slow destruction" simulations for the particular model boxes in which the monitoring stations are located.

4.2.1. Vertical profiles. In Figure 5 we compare both the "slow destruction" and "fast destruction" simulations of vertical profiles in \bar{R}_{O_3} and \bar{V}_t with observation. \bar{V}_t is the yearly average of V_t , the percent standard deviation calculated relative to the local monthly mean mixing ratio, and is a measure of the local temporal variability. It is calculated for a particular grid point from the local time series and is strongly influenced by transient eddy processes. The most extensive ozonesonde data sets available from a station in each of the major latitude regions are used. With only 43 ozonesondes from Natal and only 45 from Panama, yearly average profiles are used. There are insufficient data to construct profiles from the southern hemisphere subtropics and polar region. The northern hemisphere subtropics are discussed in section 4.2.2 (see Figure 11).

The shapes of the simulated profiles of R_{O_3} are in qualitative agreement with observation for all stations except Natal. While the simulated profiles for Natal and Panama are quite similar, the observations differ greatly. The observed Natal profile increases much more rapidly with height and exceeds the "slow destruction" upper limit above 500 mbar. If more extensive measurements support these differences between the

northern hemisphere and southern hemisphere tropics and if NO_x is low as it was for the October flight [*Gregory et al., 1984*], a significant defect in the model's tropical transport, both tropospheric and stratospheric, will have been exposed. With the exceptions of the northern hemisphere high-latitude station at Resolute and the tropical station at Natal, the measured profiles are bracketed by the two simulations. The excess O₃ at northern hemisphere high latitudes has already been discussed in section 4.1. However, at Resolute, where W_0 has the ice value (0.1 or 0.02) for the two integrations, the simulated and observed vertical gradients are in agreement. Over continental regions where W_0 is high (1.0 or 0.2), the simulated R_{O_3} profiles decrease much more sharply in the boundary layer. Unlike the overall profile, the tropopause height is well simulated in the tropics with the sharp increase occurring at a lower height over Natal, just as observed. However, at mid-latitudes in both hemispheres the simulated sharp increase occurs higher than observed.

The simulated V_t profiles are also in qualitative agreement with observation. Because the simulated variability lacks contributions from interannual time scales, diurnal and shorter time scales, and experimental error, it should be less than observed. When the simulated lower limit of V_t ("slow destruction") exceeds observations, we suspect errors in the simulation, though a systematic error in the measurement technique or the data treatment is still possible. As previously observed by *Pittock* [1977] in his analysis of the Aspendale data, V_t is a maximum in the boundary layer and the tropopause region and a minimum in the free troposphere. Associated with the steep simulated boundary layer gradient in R_{O_3} over continental sites is a large value of V_t at the surface which may exceed observation (for example, Wallops Island). At mid- and high latitudes the increase in V_t in the tropopause region occurs higher than observed and has a significantly smaller value.

While the simulated and observed profiles of R_{O_3} and V_t are in qualitative agreement, there are two regions of significant disagreement: the continental boundary layer where W_0 is relatively fast and the tropopause region at mid- and high latitudes.

Three explanations for the model's exaggerated vertical gradients and surface variability in the continental boundary layer are lack of photochemistry, lack of a seasonal cycle in W_0 , and weak vertical mixing in the model's boundary layer. As observed in section 3.1 (see Figure 1) the deep minimums at the surface over land are most extreme in the winter. While photochemistry would certainly work to fill the minima over land, during the winter when the need is greatest it will have little effect. The second possibility is the lack of seasonal dependence in W_0 . One would expect the deposition velocity to decrease considerably over land in the mid- and high latitudes during winter, particularly with snow cover [*Wesely et al., 1981*]. The third possibility is the model's transport in the boundary layer. The lack of diurnal forcing in the model's boundary layer may understate the mixing between the bottom two levels. At this time all three (photochemistry, seasonal W_0 , and boundary layer mixing) may be responsible. With regard to the observations, daytime ozonesonde measurements exclude the steepest gradients which normally occur at night, and the lack of vertical resolution in the reported measurements further decreases the slope.

The simulated sharp increase in R_{O_3} and the maximum in V_t in the region of the tropopause occur significantly higher than observed for mid- and high latitudes. This may be due to both

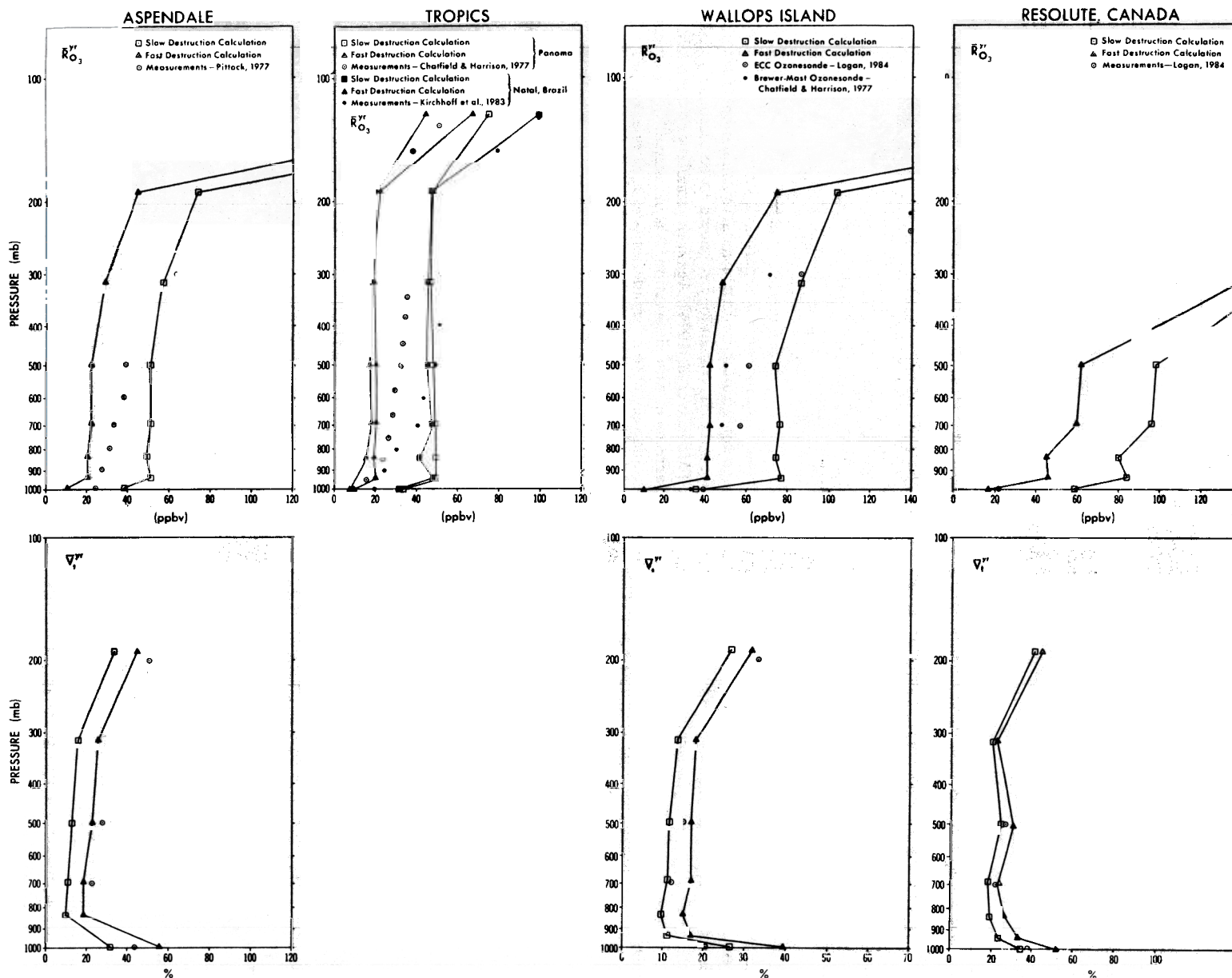


Fig. 5. Vertical profiles of yearly averaged ozone mixing ratios at standard heights as well as the corresponding yearly average of the monthly percent standard deviations are taken from multiyear ozonesonde records of selected observing stations and compared with model results from the same locations.

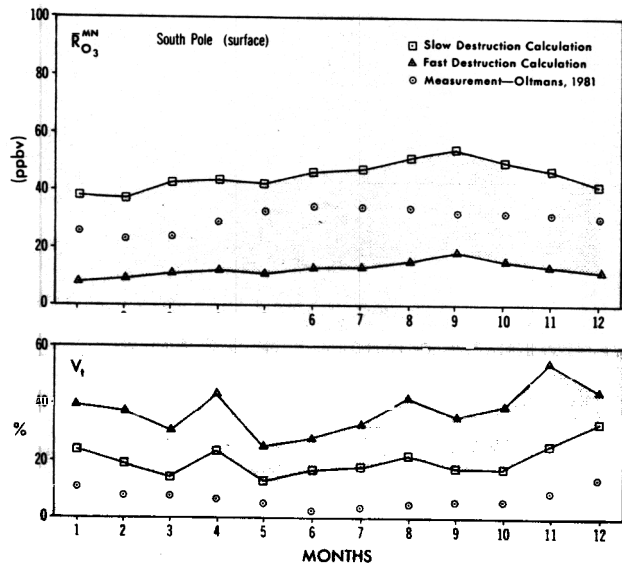


Fig. 6. Monthly averages of a multiyear continuous time series from the south pole [Oltmans, 1981] are compared with the monthly averages of the two model simulations taken from the same location. Both observed and simulated percent standard deviations calculated relative to respective monthly mean mixing ratios are plotted in the lower graph.

dynamical defects and coarse vertical resolution in the parent GCM which cause the simulated tropopause to form higher than observed at mid- and high latitudes. This same lack of vertical resolution should also reduce the smaller-scale fluctuations in that region and lead to a significant underestimation of V_i as is also shown in Figure 5.

The explanation for the apparently anomalous behavior of the Natal data is not obvious. While absolute differences might be explained by calibration differences between Brewer-Mast and ECC sondes, the observed vertical profiles, unlike the simulations, have different slopes in the troposphere. It is possible that the same atmospheric transport processes which produce the large ozone values at 500 mbar over the southern hemisphere tropics in October (see Figure 4) are responsible.

4.2.2. Time series. In this section we will compare the seasonal cycles of simulated and observed monthly mean ozone mixing ratios $\bar{R}_{O_3}^{mn}$ as well as percent standard deviations relative to the monthly means V_i . The observed monthly means and percent standard deviations are local multiyear averages, depending on the length of the time series, while the simulated values are for a single model year from the model grid box containing the station. Although there is significant interannual variability in the real atmospheric circulation, the variance analysis by Pittock [1977] found that for tropospheric ozone over Aspendale the dominant time scales of fluctuations are seasonal or shorter.

The south pole surface data of Oltmans [1981] are compared with the simulations in Figure 6. The observed monthly means and amplitude of seasonal oscillation are bracketed by the model results. While both the simulations and observations have a southern hemisphere summer minimum, the observations have a broad June–August maximum and the simulations have one in September. An earlier 5-year surface data set using a less accurate sensor [Oltmans and Komhyr, 1976] did find an August–September maximum. The model V_i are much larger than observed.

Twelve years of Brewer-Mast ozonesonde data from Aspendale, Australia (38°S, 145°E), which have been analyzed by

J. A. Logan (manuscript in preparation, 1984) are compared with the local simulated seasonal cycles of $\bar{R}_{O_3}^{mn}$ and V_i at 500 mbar in Figure 7. For $\bar{R}_{O_3}^{mn}$ we have excellent agreement between the simulations and observation with the exception of an apparent 1-month phase shift between the seasonal cycles. Similar agreement is found for other tropospheric levels. Simulated and observed V_i are of the same magnitude, though the observed values show a slight seasonal cycle with a February–March maximum.

Observational data from a surface monitoring station in Cape Grim, Tasmania (41°S, 145°E), were provided by I. E. Galbally (private communication, 1984) and are compared with model results in Figure 8. The upper and lower limit model simulations of $\bar{R}_{O_3}^{mn}$ bracket the measurements and they all have a January–February minimum. However, the observed seasonal cycle is similar to that seen at the south pole with a broad maximum from June to September, while the maxima for both simulations occur later. The observed southern hemisphere winter maximum (June–September) may result from a large seasonal decrease in photochemical destruction. However, NO_x measurements are not available for Cape Grim.

Four years of surface ozone measurements from Samoa (14°S, 171°W) [Oltmans, 1981] are compared with the model in Figure 9. While this is boundary layer data, the deposition velocity is low over the ocean, and the surface is uniform on a large scale. Thus the model's simulation of the atmospheric boundary layer over sea is expected to be much better than it is over land. Furthermore, the model's simulation of tropical and subtropical climatology is known to be reasonably accurate [Manabe et al., 1974]. Again the simulation is in qualitative agreement with observation. V_i is bracketed by the simulations, and they have no significant seasonal cycle. While $\bar{R}_{O_3}^{mn}$ is bracketed by the model simulations, the maxima differ by 1–2 months, the observed values are very close to the "fast destruction" limit ($W_0 = 0.1 \text{ cm s}^{-1}$ over the ocean) and the

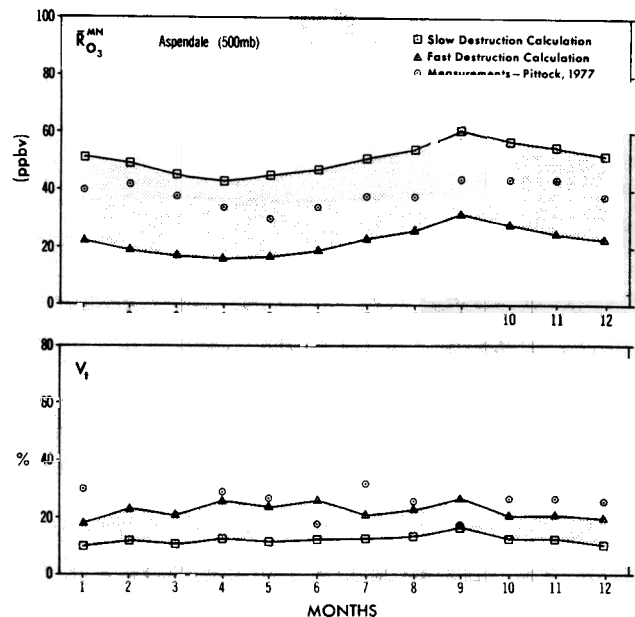


Fig. 7. Monthly mean ozone mixing ratios from the 500-mbar layer of the multiyear Brewer-Mast ozonesonde record measured in Aspendale, Australia [Pittock, 1977], are compared with the model data taken from the 500-mbar box over Aspendale. The local percent standard deviations for both the observations and simulated data are presented in the lower graph.

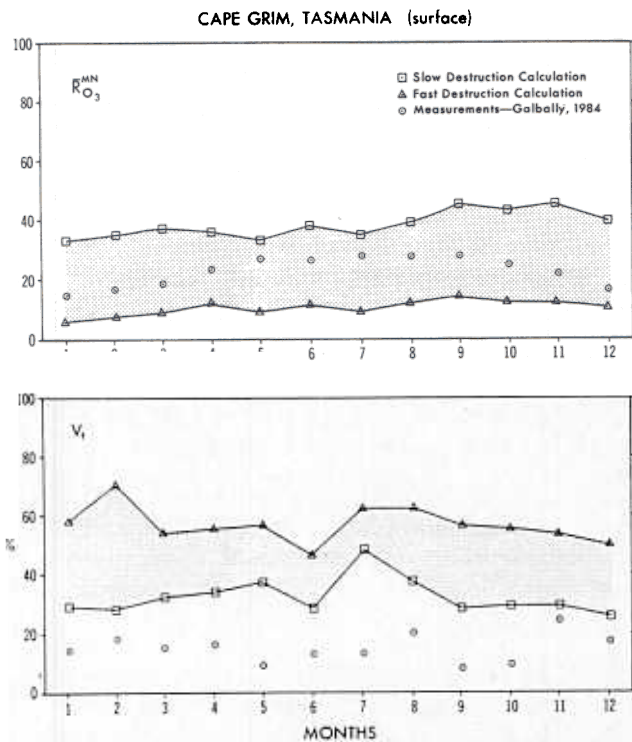


Fig. 8. Monthly averages of the multiyear continuous surface time series measured at Cape Grim, Tasmania (I. E. Galbally, private communication, 1984) as well as the percent standard deviations relative to those observed monthly means are compared with data from both the “fast destruction” and “slow destruction” simulations which were taken from the model box containing Cape Grim.

observed seasonal amplitude is larger. A correct simulation would require an additional surface destruction process. Photochemical destruction [e.g., Fishman et al., 1979], which has been identified in the equatorial Pacific by Liu et al. [1983], is a possibility if the NO_x concentration is low enough. While measurements for Samoa are not available,

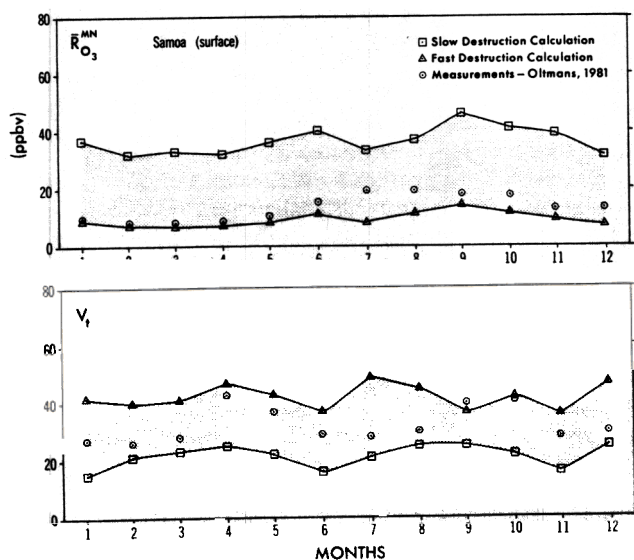


Fig. 9. Monthly averages of the multiyear continuous surface time series measured on Samoa [Oltmans, 1981] and the percent standard deviations of the observations are compared with model data taken from the box containing Samoa for both simulations, “fast destruction” and “slow destruction.”

McFarland et al. [1979] have found very low values in the tropical Pacific.

Observations from the surface station on Mauna Loa, Hawaii (20°N , 156°W), were selected for times known to have downslope winds and are thought to be representative of 680 mbar. In Figure 10, we see that both $\bar{R}_{\text{O}_3}^{\text{MN}}$ and V_t are well bracketed by the simulations. The observed seasonal cycle for $\bar{R}_{\text{O}_3}^{\text{MN}}$ is qualitatively reproduced by the model. Both the simulated and measured time series have similar maxima and amplitude, but the simulated minimum occurs 3 months later than the observed. The observed V_t has a slight August maximum, while the model produces a slight minimum. As in the Samoa data, the observed mixing ratios are close to the “fast destruction” limit. While even the downslope wind may have some contact with the surface above the Mauna Loa measurement site, there is little, if any, vegetation; thus surface removal should not be a factor. Although the low NO_x concentrations needed to support photochemical destruction of O_3 in the boundary layer have only been observed in a few isolated instances, much of the tropical and subtropical boundary layer may require both surface deposition and net photochemical destruction.

Monthly mean ozone mixing ratios from 69 ozonesondes taken in the Bahamas (21.5°N , 70°W) over a 4-year period by Hering and Borden [Chatfield and Harrison, 1977] are compared with the simulations in Figure 11. Figure 11 clearly demonstrates the variety of seasonal behavior in the troposphere that can result from transport mechanisms alone (without the benefit of in situ chemistry). At the surface the observations are well bracketed by the simulations and all have similar maxima, minima, and relative amplitudes. Moving up through the troposphere, the observed minimum stretches from fall to fall-winter and the spring maximum changes to a double spring-summer maximum and finally to a simple summer maximum in the upper troposphere. The “fast destruction” and “slow destruction” simulations bracket this behavior at all levels and reproduce the observed minima quite well. However, the model maxima, while qualitatively similar, are stronger in the spring and weaker in the summer.

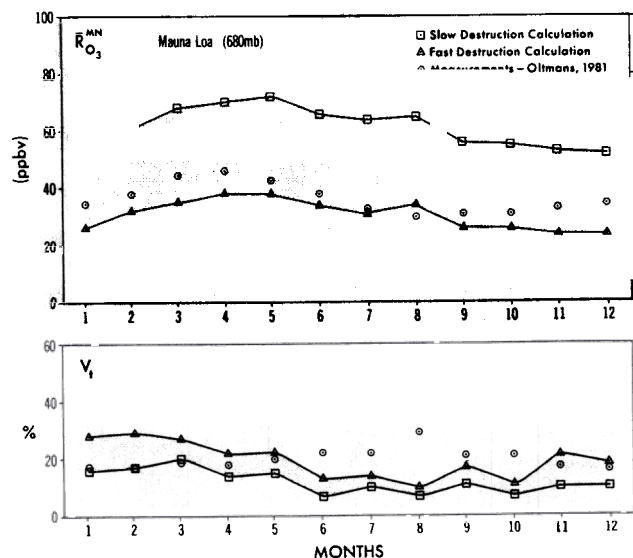


Fig. 10. Monthly averages of the multiyear surface time series measured at Mauna Loa, Hawaii, under downslope conditions [Oltmans, 1981] and the corresponding percent standard deviations are compared with model data taken from the 685-mbar model box over Hawaii.

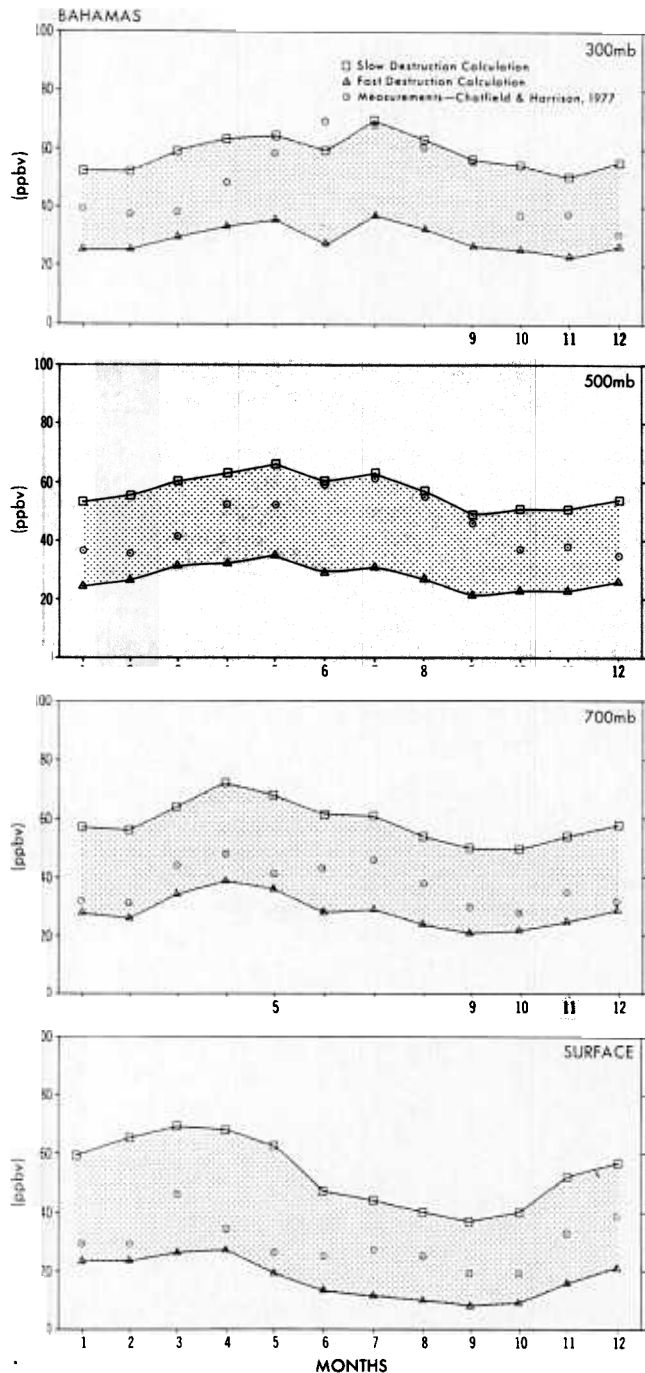


Fig. 11. Monthly mean ozone mixing ratios calculated from the 3-year Brewer-Mast ozonesonde record measured at Grand Turk, Bahamas [Chatfield and Harrison, 1977], are compared with model results (both "fast destruction" and "slow destruction") from the same location. This comparison is made for four levels in the troposphere; the surface, 700, 500, and 300 mbar.

Furthermore, the simulated amplitude of seasonal variation is significantly less than observed at 500 and 300 mbar.

The spring maximum at the surface is the result of strong equatorward-downward transport in the spring which has been previously observed, via nuclear debris, in both the model and the real atmosphere (MM78). In the summer an upper tropospheric trough or low, which normally forms over the subtropical Atlantic in both the model and real atmosphere, serves to transport higher O_3 mixing ratios from mid-latitudes down to the subtropical Atlantic. This can be clearly

seen in the 190-mbar panels of Figure 1. However, such behavior is very sensitive to the exact location of the upper troposphere trough and to the particular summertime meteorology at mid-latitudes. Therefore quantitative agreement would be fortuitous. Ozone production, driven by transported mid-latitude NO_x , is also a potential explanation for the strong summer peak at 500 mbar and above. Note that the observed values, unlike the previous two figures, are significantly above the fast destruction limit. Higher NO_x levels over the Atlantic than over the Pacific are supported by some recent simulations we have performed for a North American combustion source of NO_x . However, the few NO_x measurements from the subtropical Atlantic (A. L. Torres, private communication, 1983) are quite low.

The two major disagreements between the observed and simulated ozone behavior in the "free troposphere" occur at mid- and high northern hemisphere latitudes as shown in the 500-mbar time series presented in Figure 12. While the more recent ECC measurements at Wallops Island ($38^\circ N, 27^\circ W$) have a larger seasonal amplitude in \bar{O}_3 than the earlier Brewer-Mast time series, they both show a June–July maximum and winter minimum. The two simulations, while still bracketing the observations, show a broad February–June maximum and late summer–early fall minimum. The Brewer-Mast time series from Hohenpeissenberg ($47.5^\circ N, 11^\circ E$) and Payerne ($46.5^\circ N, 7^\circ E$) are in excellent agreement at 500 mbar with a June–July maximum and winter minimum. The upper and lower limit simulations only partially bracket the observations and have an April maximum and September minimum. The observed 500-mbar time series at Resolute, Canada ($74^\circ N, 95^\circ W$), again shows a June maximum and December–January minimum, while the simulated time series have broad February–May maxima, August–December minima, and no longer bracket observation. We have already discussed the excess O_3 at high latitudes in the transport simulations (section 4.1) and will now concentrate on the seasonal cycle.

It is clear that the observed and simulated seasonal cycles are approximately 3 months out of phase in the "free troposphere." A harmonic analysis of 15 mid- and high latitude ozonesonde data sets by J. London (private communication, 1983) finds the 500-mbar seasonal maxima consistently in June–July, while the model maxima for the same locations range from January to May with most occurring in March. However, no observational data exist for oceanic sites, though Resolute is in clean air. In the tropopause region and in the lower stratosphere, the simulated seasonal cycles are in good agreement with the analysis by J. London (private communication, 1983). Three possible explanations for the disagreement in the "free troposphere" are the lack of tropospheric chemistry, deficiencies in model transport, and systematic error in the observations.

The observed maxima and minima appear to support a chemically driven summertime net production and wintertime net destruction. However, while the time averages of the multiyear time series show smooth June–July maxima, they also display considerable interannual variability with individual yearly maxima ranging from April to August. Such variability is not consistent with photochemical control driven only by the seasonal variation in solar flux and strongly argues for at least the transport control of one or more chemical precursors of ozone. The possible role of chemistry in the summer maxima and a possible indirect NO_x transport mechanism will be discussed in detail in section 5.

While model transport has produced 500-mbar summer

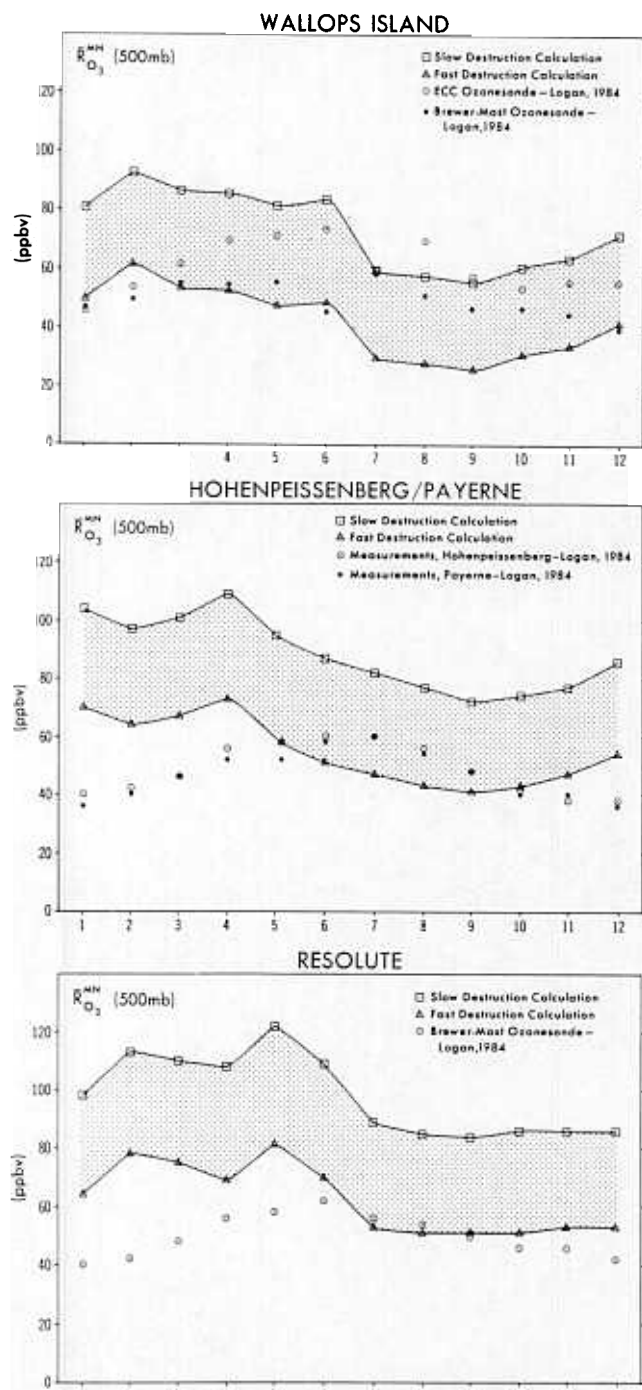


Fig. 12. Monthly averages of the 500-mbar multiyear ozonesonde records from four northern continental stations (Wallops Island, Virginia; Hohenpeissenberg, Germany; Payerne, Switzerland; and Resolute, Canada) are compared with the 500-mbar results of both the "fast destruction" and "slow destruction" simulations. The simulated results are taken from boxes in the model which lie over the ozonesonde stations.

maxima in the subtropics (see Figure 11) and at the pole (see Figure 2), no obvious atmospheric transport process would appear to explain a summer maximum throughout the mid- and high latitudes of the northern hemisphere. Although defects in the model transport are strongly implied in the excess O_3 at high latitudes, we find no obvious defect in the model's dynamics which would explain such a large-scale disagreement between observed and simulated seasonal cycles. The

apparent late spring maximum in ^{90}Sr deposition [Staley 1982; Fabian, 1973] does suggest some role for transport, though it does not explain a June maximum in O_3 . Furthermore, ^{90}Sr is strongly influenced by seasonal patterns of precipitation [Staley, 1982]. It is not clear what, if anything, can be inferred about the seasonal cycle in O_3 from the ^{90}Sr data. The possibility of systematic measurement error among a number of different devices appears quite unlikely. The observed and simulated seasonal time series of V_t , while not shown in Figure 12, are in qualitative agreement and offer no clues regarding the source of the disagreement.

As mentioned in the introduction, we do not expect the global transport model to simulate ozone accurately in the continental boundary layer, where subgrid scale transport processes, highly variable surface removal, and an active and fluctuating pollution chemistry are all important. However, much of the best data come from just such sites. In Figure 13 we examine surface time series at the three previously discussed ozonesonde stations as well as two continuous surface ozone time series from the Boulder area (40°N , 105°W) [Oltmans, 1981; Fehsenfeld et al., 1983]. While all observed time series from mid-latitude show a summer maximum and four of the five show a winter minimum, there are large differences in the nature and amplitude of the seasonal cycles. In the Boulder area the observed ozone exceeds or equals the upper limit simulation throughout the year. Furthermore, while the simulations have definite spring maxima and fall minima, the observations of Oltmans [1981] show a series of small maxima and minima while the data of Fehsenfeld et al. [1983] are essentially flat with a weak maximum in March and another in July. For Wallops Island, the simulated and observed R_{O_3} maxima are similar, though the seasonal amplitudes differ and the ECC data exceed the upper limit of the model. In Hohenpeissenberg and Payerne the observed seasonal structure again differs a great deal from the simulation. Photochemistry has already been shown to influence the Niwot data in the Boulder area [Fehsenfeld et al., 1983], though the model's weak boundary layer mixing and lack of a seasonal dependence in W_0 are also a factor at all the sites.

At Point Barrow (71°N , 157°W) the model simulations and the continuous surface time series of Oltmans [1981L] are completely out of phase. It would appear that in winter a W_0 of 0.02 cm s^{-1} is appropriate and that in summer a value of 0.1 cm s^{-1} is needed. This suggests either a role for photochemical destruction at the surface as previously mentioned by Oltmans [1981] or a strong seasonal dependence in W_0 . The observed V_t also differ significantly from the simulation, with very low observed values in the winter and a sharp spring maximum. The simulated V_t are, except for the spring, much larger and show a winter maximum. The winter maximum in observed $R_{O_3}^{\text{mm}}$ and winter minimum in observed V_t are found at both Point Barrow and Resolute [Oltmans, 1981]. It should be noted that the observed seasonal cycle for surface ozone at Resolute is completely out of phase with the observed seasonal cycle at 500 mbar. Obviously, a simple chemical production driven by surface sources is not the answer.

As expected, with the exception of what is probably fortuitous agreement at Wallops Island, there is little similarity between observation and simulation in the continental boundary layer.

5. ROLE OF CHEMISTRY

In this section we will examine the role of chemistry in the ozone continuity equation (see equation (1) in section 2) and

SURFACE OBSERVATIONS AND SIMULATIONS

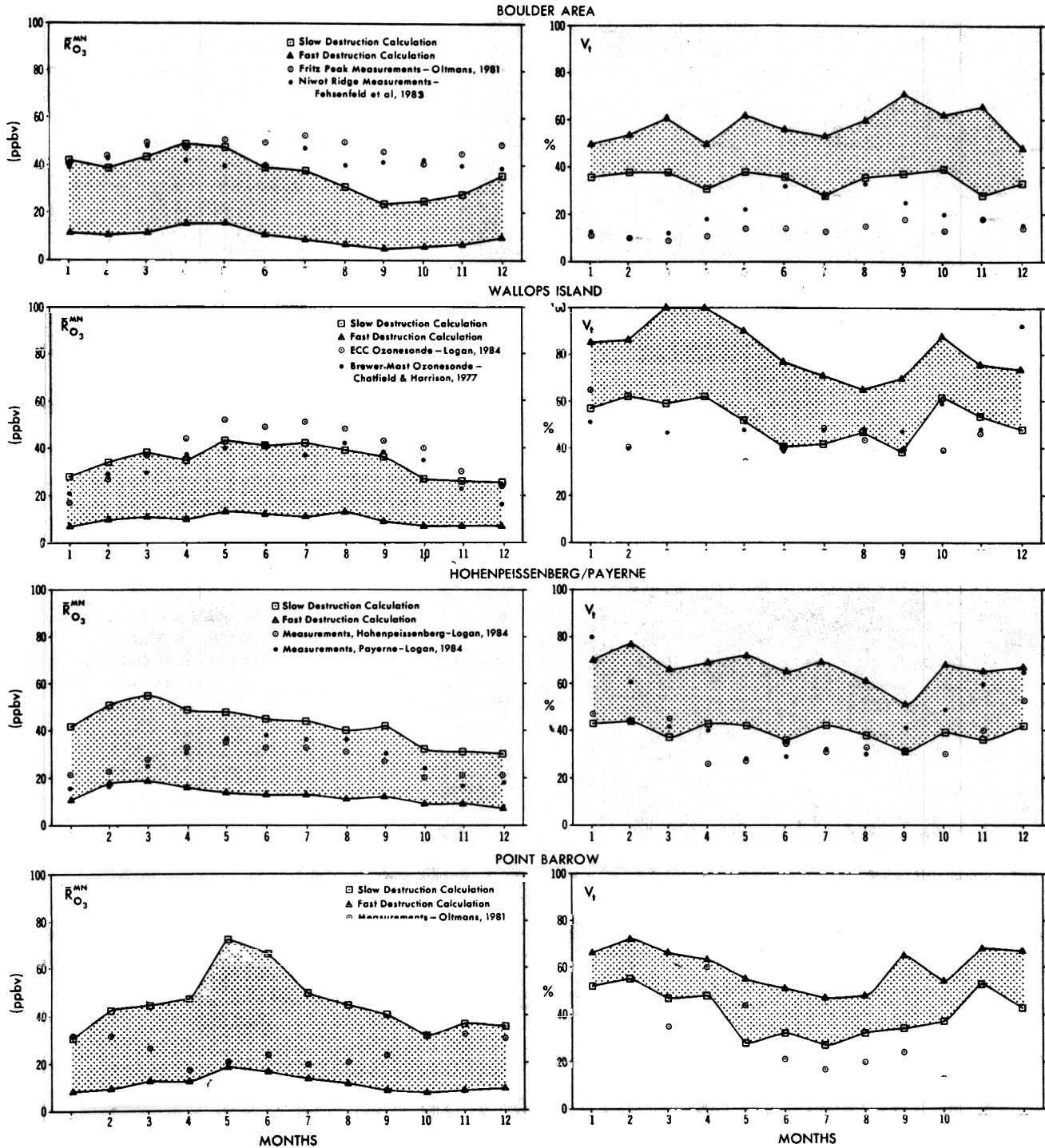


Fig. 13. Monthly averages from the surface multiyear ozonesonde records of four stations (Wallops Island, Virginia; Hohenpeissenberg, Germany; Payerne, Switzerland; and Point Barrow, Alaska) as well as from two continuous surface multiyear time series near Boulder, Colorado, are compared with monthly averages generated by the "fast destruction" and "slow destruction" simulations. The model data are taken from model boxes containing the observation sites. In the right half of the figure, the corresponding observed and simulated percent standard deviations are compared.

determine the potential local impact of chemistry on those disagreements between transport simulation and observation which have been identified in section 4.

5.1. Conceptual Framework

We will consider the clean "free troposphere," which consists of O_3 , H_2O , CO , CH_4 , NO , NO_2 , NO_3 , N_2O_5 , and

HNO_3 . The rapid removal of O_3 and soluble NO_x species by surfaces can be ignored and the " CH_4 oxidation cycle" has been removed to simplify the equations. This does not result in any qualitative change in either the following discussion or the calculated chemical tendencies. The relevant reactions are given in Table 1.

For purposes of discussing O_3 production and destruction,

TABLE 1. Tropospheric Reactions

Reaction	Notation*	Units	Remarks
(R1) $O_3 + hv \rightarrow O(^3P) + O_2$	$J_1 = 14.4^{-4}$	s^{-1}	noontime values at 45°N and 500 mbar for day 173†
(R2) $O_3 + hv \rightarrow O(^1D) + O_2$	$J_2 = 3.1^{-5}$	s^{-1}	noontime values at 45°N and 500 mbar for day 173†
(R3) $O(^3P) + O_2 + m \rightarrow O_3 + m$	$k_3 = 6.2^{-34}(300/T)^{-2}$	$cm^6 \text{ molecule}^{-2} s^{-1}$	WMO/NASA [1981]
(R4) $O(^3P) + O_3 \rightarrow 2O_2$	$k_4 = 1.5^{-11} \exp(-2200/T)$	$cm^3 \text{ molecule}^{-1} s^{-1}$	WMO/NASA [1981]
(R5) $O(^1D) + m \rightarrow O(^3P) + m$	$k_5 = 3.04^{-11}$	$cm^3 \text{ molecule}^{-1} s^{-1}$	Hampson [1980]
(R6) $O(^1D) + H_2O \rightarrow 2OH$	$k_6 = 2.3^{-10}$	$cm^3 \text{ molecule}^{-1} s^{-1}$	Hampson [1980]
(R7) $O_3 + NO \rightarrow NO_2 + O_2$	$k_7 = 3.8^{-12} \exp(-1580/T)$	$cm^3 \text{ molecule}^{-1} s^{-1}$	WMO/NASA [1981]
(R8) $HO_2 + NO \rightarrow NO_2 + OH$	$k_8 = 8.5^{-12}$	$cm^3 \text{ molecule}^{-1} s^{-1}$	Hampson [1980]
(R9) $NO_2 + hv \rightarrow NO + O$	$J_9 = 8.9^{-3}$	s^{-1}	Parrish et al. [1983]
(R10) $OH + NO_2 + m \rightarrow HONO_2 + m$	$k_{10} = 1.1^{-11}$	$cm^3 \text{ molecule}^{-1} s^{-1}$	Hampson [1980]
(R11) $HNO_3 + hv \rightarrow OH + NO_2$	$J_{11} = 6.9^{-7}$	s^{-1}	noontime values at 45°N and 500 mbar for day 173†
(R12) $HNO_3 \rightarrow$ wet and dry removal	$k_{12} = 3.5^{-7}$	s^{-1}	a parameter which was chosen to give a 1-month lifetime
(R13) $OH + HNO_3 \rightarrow H_2O + NO_3$	$k_{13} = 9.4^{-15} \exp(778/T)$	$cm^3 \text{ molecule}^{-1} s^{-1}$	Hampson [1980]
(R14) $O_3 + NO_2 \rightarrow NO_3 + O_2$	$k_{14} = 1.2^{-13} \exp(-2450/T)$	$cm^3 \text{ molecule}^{-1} s^{-1}$	WMO/NASA [1981]
(R15) $NO_3 + hv \rightarrow NO_2 + O(A)$ or $NO + O_2(B)$	$J_{15a} = 6.2^{-2}$ $J_{15b} = 6.2^{-3}$	s^{-1}	noontime values at 45°N and 500 mbar for day 173†
(R16) $NO_3 + NO_2 \rightarrow N_2O_5$	$k_{16} = 1.5^{-13} \exp(861/T)$	$cm^3 \text{ molecule}^{-1} s^{-1}$	Hampson [1980]
(R17) $N_2O_5 \rightarrow NO_3 + NO_2$	$k_{17} = 1.24^{14} \exp(-10,317/T)$	$cm^3 \text{ molecule}^{-1} s^{-1}$	Hampson [1980]
(R18) $N_2O_5 + hv \rightarrow NO_3 + NO_2$	$J_{18} = 3.5^{-5}$	s^{-1}	noontime values at 45°N and 500 mbar for day 173†
(R19) $OH + CO \xrightarrow{O_2} CO_2 + HO_2$	$k_{19} = 1.35^{-13} (1 + P)$	$cm^3 \text{ molecule}^{-1} s^{-1}$	WMO/NASA [1981]
(R20) $OH + O_3 \rightarrow HO_2 + O_2$	$k_{20} = 1.6^{-12} \exp(-940/T)$	$cm^3 \text{ molecule}^{-1} s^{-1}$	WMO/NASA [1981]
(R21) $HO_2 + O_3 \rightarrow OH + 2O_2$	$k_{21} = 1.4^{-14} \exp(-580/T)$	$cm^3 \text{ molecule}^{-1} s^{-1}$	WMO/NASA [1981]
(R22) $OH + OH \rightarrow H_2O + O$	$k_{22} = 4.5^{-12} \exp(-275/T)$	$cm^3 \text{ molecule}^{-1} s^{-1}$	WMO/NASA [1981]
(R23) $OH + OH + M \rightarrow H_2O_2 + M$	$k_{23} = 2.5^{-31}(300/T)^{-0.8}$	$cm^6 \text{ molecule}^{-2} s^{-1}$	Hampson [1980]
(R24) $OH + HO_2 \rightarrow H_2O + O_2$	$k_{24} = 2.0^{-10}$	$cm^3 \text{ molecule}^{-1} s^{-1}$	Hampson [1980]
(R25) $HO_2 + HO_2 \rightarrow H_2O_2 + O_2$	$k_{25} = 4.75^{-14} \exp(1150/T)$	$cm^3 \text{ molecule}^{-1} s^{-1}$	Hampson [1980]
(R26) $OH + H_2O_2 \rightarrow H_2O + HO_2$	$k_{26} = 3.1^{-12} \exp(-187/T)$	$cm^3 \text{ molecule}^{-1} s^{-1}$	Hampson [1980]
(R27) $H_2O_2 + hv \rightarrow 2OH$	$J_{27} = 3.1^{-6}$	s^{-1}	noontime values at 45°N and 500 mbar for day 173†
(R28) $H_2O_2 \rightarrow$ wet and dry removal	$k_{28} = 3.5^{-7}$	s^{-1}	a parameter which was chosen to give a 1-month lifetime

*The exponent specifies the power to 10 by which each entry is to be multiplied.

†Photodissociation rates were calculated with equation (1) by Levy [1974] with the added assumption of no aerosol or Raleigh scattering. See MLM80 for details on solar flux and absorption coefficients.

it is conceptually convenient to regard HO_x radicals as $\frac{1}{2}O_3$. This is one step further than the inclusion of reactive nitrogen, O_3 , $O(^3P)$, and $O(^1D)$ as O_x [Liu, 1977]. Therefore we will consider available O_3 as

$$O_x = O_3 + O(^3P) + O(^1D) + \frac{1}{2}OH + \frac{1}{2}HO_2 + H_2O_2 + NO_2 + 2NO_3 + 3N_2O_5 + \frac{3}{2}HNO_3 \quad (3)$$

The production and loss terms then become relatively straightforward:

$$P(O_x) = k_8 n(OH) n(NO) \quad (4)$$

and

$$L(O_x) = n(O_3)[k_{20}n(OH) + k_{21}n(HO_2)] + [0.5k_{12}n(HNO_3) + k_{24}n(OH)n(HO_2) + k_{26}n(OH)n(H_2O_2) + k_{28}n(H_2O_2)] + [2J_{15b}n(NO_3) + k_{12}n(HNO_3) + 3k_{12}n(N_2O_5)] \quad (5)$$

In $L(O_x)$ the first line represents the direct destruction of O_3 , the second line represents indirect destruction via the loss of HO_x radicals, and the third line represents the indirect

destruction via the loss of oxidized reactive nitrogen species. The production term involves the oxidation of NO to NO_2 without loss of O_x . In the surface layer we would include CH_3O_2 , CH_3O , H_2CO , and CH_3O_2H in equations (3)–(5) and would include an extra term in $L(O_x)$, surface deposition of O_3 , which would dominate. This would not change the basic concepts behind $P(O_x)$ and $L(O_x)$. A lower limit estimate of the magnitude of $L(O_x)$ can be made without the detailed NO_x and HO_2 information needed to calculate $P(O_x)$. While the radical sink terms in the second line of $L(O_x)$ are difficult to calculate separately, at steady state their sum plus the very small contribution from reaction (R22) must equal the production given by (R6). Provided that the O_3 and H_2O distributions are known, the radical production rate can be easily estimated. Liu et al. [1980] report a global average column rate of $1.9 \times 10^{11} \text{ molecules cm}^{-2} s^{-1}$ which is almost 4 times the model's O_3 flux from the stratosphere. While there is still considerable uncertainty in the global distribution of O_3 and H_2O , this estimate should be qualitatively correct. This result suggests that the globally averaged influence of photochemistry is at least comparable to, if not significantly larger than, the contribution from transport.

5.2. Chemical Tendency

Estimates of either globally averaged or column production and destruction rates are not very relevant to understanding

TABLE 2. Specified Conditions for 45°N at 500 mbar

	Temperature, °C	Total O ₃ , molecules cm ⁻²	H ₂ O (Mixing Ratio)	CO (Mixing Ratio)	Day
Winter	246	8.4 ¹⁸	0.7 ⁻³	1.5 ⁻⁷	
Spring	251	9.4 ¹⁸	0.9 ⁻³	1.5 ⁻⁷	
Summer	261	8.2 ¹⁸	1.9 ⁻³	1.5 ⁻⁷	
Fall	254	7.3 ¹⁸	1.2 ⁻³	1.5 ⁻⁷	

The exponents indicate the power of 10 by which each entry is to be multiplied.

the three-dimensional behavior of tropospheric O₃. The two local chemical issues are the sign of the chemical tendency ($Pp_* - Lp_*R$) in equation (1) of section 2 and its magnitude. To consider both the direct chemical effects on the local tendency and the indirect chemical influence through modification of the local transport terms (particularly under conditions of strong vertical mixing), a full three-dimensional transport chemical study is required. Prior to such a complex study, we wish to identify the direct role of chemistry in the local continuity equation.

Tropospheric NO_x is highly variable in space and time, and its global distribution is not known. Therefore we examine the O₃ chemical steady state and net chemical tendency in the "free troposphere" over a wide range of NO_x mixing ratios. Nonlinear differential equations describing the diurnal time dependent behavior of $n(\text{O}_3 + \text{O})$, $n(\text{NO})$, $n(\text{NO}_2)$, $n(\text{NO}_3)$, $n(\text{N}_2\text{O}_5)$, $n(\text{HNO}_3)$, $n(\text{HO})$, $n(\text{HO}_2)$, and $n(\text{H}_2\text{O}_2)$ are integrated until their diurnal cycles are in steady state (≈ 100 days). The equations are integrated for NO_x = NO + NO₂ + NO₃ + 2N₂O₅ ranging from 1 ppt to 500 pptv. This range of NO_x integrations is performed at 500 mbar for each of the four seasons. The climatic values of temperature, total column ozone above 500 mbar, H₂O, and CO are specified (see Table 2).

Plots of the diurnal averaged steady state values of R_{O₃} as a function of R_{NO_x}, the mixing ratio of the sum of all the rapid interchangeable nitrogen species, are shown in Figure 14 for the four seasons. While the four curves have slightly different shapes, the dominant factor is R_{NO_x}. The differences in temperature, photodissociation rates, and R_{H₂O} have smaller effects and tend to cancel. For R_{NO_x} levels >100 ppt, the corresponding steady state values of R_{O₃} significantly exceed observations regardless of time of year. Therefore, if tropospheric ozone is in photochemical steady state at 500 mbar, the R_{NO_x} is constrained to a narrow range (20–70 pptv) and quite low values overall.

In Figure 15 we show O₃ chemical tendency as a function of NO_x for a range of O₃ mixing ratios. Unlike the steady state values of O₃, the chemical tendencies have a very strong seasonal dependence with maximum values as low as ± 0.3 ppb d⁻¹ in the winter and as high as ± 5.0 ppb d⁻¹ in the summer. This is not at all surprising since the strength of the chemical tendency for a given value of O₃ and NO_x depends directly on the HO_x concentration which is highly seasonally dependent.

5.3. Potential Roles for O₃ Chemistry

There are four significant disagreements between the simulations and observation which might be explained by the model's lack of photochemistry: (1) the apparent need for an additional O₃ loss mechanism, corresponding to an equivalent deposition velocity of order 0.1 cm s⁻¹, in the boundary layer of the tropical and subtropical Pacific and the summertime

Arctic, (2) the exaggerated R_{O₃} gradients, low values of surface R_{O₃}, and high surface values for V_i simulated in the continental boundary layer, (3) the excess ozone in the model's northern hemisphere north of 40°N, and (4) the simulated spring maximum and fall minimum in the middle troposphere at mid- and high latitudes of the northern hemisphere in contrast to the consistent June maximum and winter minimum in observations.

Disagreements 1 and 2 are discussed briefly in section 4. The boundary layer chemistry in polluted regions is too complex for a detailed treatment in this paper, while Liu *et al.* [1983] have already discussed in detail the case for a very clean (low NO_x) boundary layer with slow surface removal. For disagreement 3 (see Figures 3 and 4) the observed values of R_{O₃} remain relatively constant north of 40°N, unlike the simulations which increase until 55°N–60°N. Furthermore, the observations fall in the range of 45–60 ppbv, which is below the simulated lower limit. In Figure 14 we find that NO_x values in the range 20–70 pptv are needed to produce chemical steady state values of R_{O₃} in the range of observations. While NO_x observations at high latitudes are limited, model simulations of the 500-mbar total reactive nitrogen (NO_y) mixing ratios resulting from stratospheric injection [Levy *et al.*, 1980] may support NO_x levels of 20–35 ppt [Liu *et al.*, 1980]. If stratospheric injection is the sole source of NO_x at 500 mbar, the resulting chemical tendency will reduce the transport excess. Unfortunately, the biggest discrepancies (see Figure 12) occur during the winter and spring when, as we can see from Figure 15, the net chemical tendency is smallest, 0.2 ppb d⁻¹ or less in winter and 0.6 ppb d⁻¹ or less in spring at 45°N. At higher latitudes there would be no chemistry in the

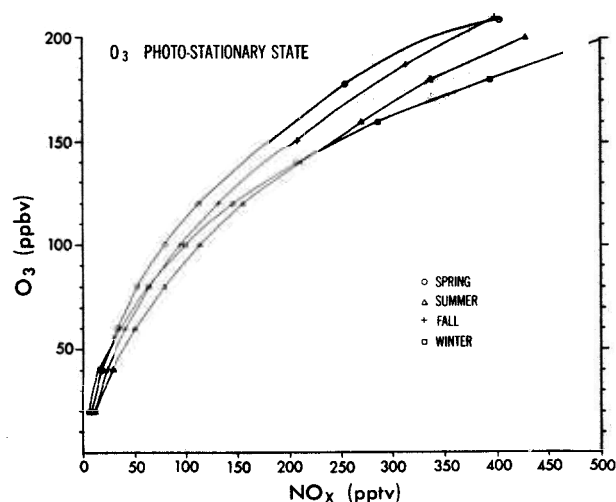


Fig. 14. The diurnal steady state O₃ mixing ratios are presented for a range of NO_x values for the four seasons.

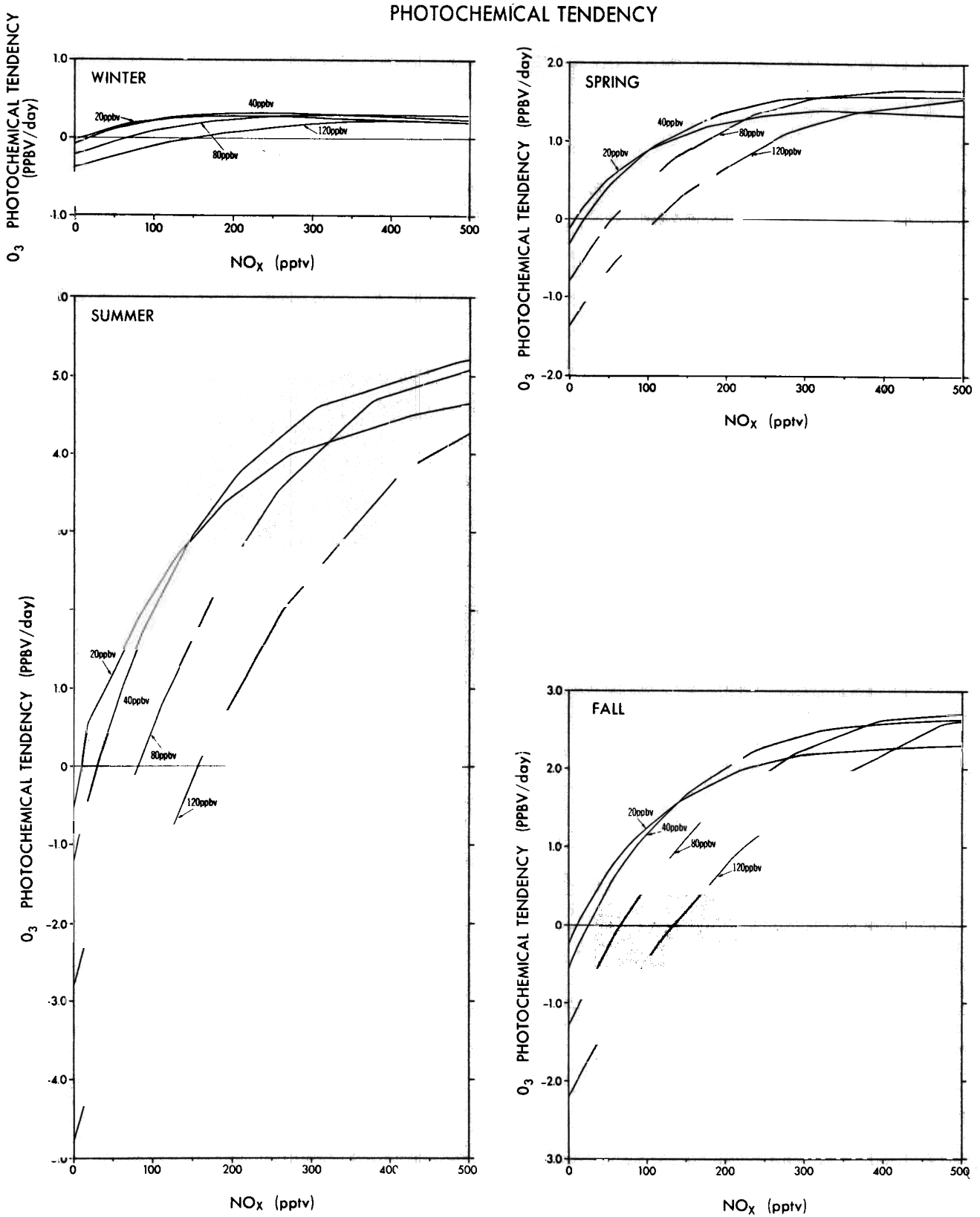


Fig. 15. Net chemical tendency calculations were performed for each of the four seasons. For each season the net ozone chemical tendency is plotted as a function of NO_x mixing ratio. Each curve represents a different specified O_3 mixing ratio in the net chemical tendency calculation.

winter and a weak tendency in the spring. While some chemical destruction may take place, it is not sufficient.

In the case of disagreement 4 (see Figure 12), the observed June–July maxima and winter minima suggest a solar flux

driven mechanism. However, the extreme interannual variability in the observed seasonal cycles clearly implies a major role for atmospheric transport, though it could be indirect transport control of the chemical precursors for ozone. With a

positive chemical tendency of 4 ppbv d^{-1} or more for $\text{NO}_x > 300 \text{ pptv}$ (see Figure 15), there may be adequate chemical production in the "free troposphere" to maintain the spring transport maximum into summer. The key, of course, is the NO_x concentration which must be raised above clean background levels which are currently believed to be much less than 300 pptv . This would require that strong summertime convection and decreased middle troposphere zonal flow more than compensate for the greatly decreased chemical lifetime of NO_x and provide a large summertime source of combustion NO_x for the "free troposphere." It can also be argued that the same strong summertime convection couples the free troposphere ozone chemistry to the very different and more active boundary layer ozone chemistry. Ultimately, the simulation in the "free troposphere" requires a full three-dimensional chemistry/transport model. However, it should be noted (see Figures 12 and 13) that the observed summertime mean monthly values at 500 mbar are $\sim 20 \text{ ppbv}$ higher than the monthly mean values in the boundary layer. At Resolute, the summer maximum at 500 mbar has become a minimum at the surface. It is not simply the export of boundary layer ozone. Something, either transport or chemistry driven, is happening in the "free troposphere" to produce both the extension of the spring maxima into summer and the positive vertical gradient.

An even more difficult issue is the observed winter minima in the "free troposphere" at mid- and high latitudes. The upper limit on wintertime tendencies at 45°N is $\pm 0.3 \text{ ppbv d}^{-1}$, though in general it would be even smaller. Furthermore, at high latitudes such as Resolute (73°N) the chemical tendency would be nonexistent. It does not seem possible that chemistry can significantly reduce the transport model's winter maximum (see Figure 12). A more likely explanation is a defect in the model's transport in the polar region. This question is being pursued with an improved general circulation/transport model.

6. SUMMARY AND CONCLUSIONS

Our long-term goal for this research is to develop an atmospheric transport chemistry model which simulates the current climatology of ozone and is able to predict its responses to perturbations, both natural and anthropogenic. The goal of this paper is to determine the role that large-scale atmospheric transport plays in the behavior of tropospheric ozone, identify potential roles for tropospheric chemistry, and gain a more global picture of tropospheric ozone. As our tools, we have used the atmospheric transport generated by a high resolution general circulation/transport model, available tropospheric ozone observations and estimates of the range of the chemical contribution to the local three-dimensional continuity equation.

We find that the transport model simulation is consistent with much that is known about tropospheric ozone: (1) The model's global mean cross-tropopause flux of $5 \times 10^{10} \text{ molecules cm}^{-2} \text{ s}^{-1}$ is in the range of previous estimates ($3\text{--}12 \times 10^{10} \text{ molecules cm}^{-2} \text{ s}^{-1}$), (2) the simulated and observed latitude gradients are in agreement from the south pole to 40°N , and (3) throughout the south pole to 40°N region, the "fast destruction" and "slow destruction" simulations qualitatively reproduce the observed seasonal cycles and bracket the observed values.

However, there are clearly a number of difficulties in the boundary layer, particularly over land: (1) The model's simu-

lation of V_t is too large over land, (2) the simulated seasonal cycle of R_{O_3} is clearly wrong over land and the simulated winter surface values are much too small, and (3) over the ocean, the low deposition velocity does not provide adequate destruction and an additional mechanism is needed. The disagreements over land are not at all surprising and appear to be the result of a number of model deficiencies: lack of chemistry, inadequate boundary layer mixing, and no seasonal dependence in the deposition velocity. The need for additional destruction over regions with a slow deposition velocity would appear to confirm the importance of photochemical destruction in such cases.

While deficiencies in the boundary layer were not unexpected, particularly over land, two major disagreements were observed in the "free troposphere": (1) North of 40°N the lower limit simulation exceeds observation by as much as 50% and the simulated latitude gradient continues to increase until 60°N , and (2) the simulated seasonal cycles have spring maxima and fall minima throughout the northern hemisphere mid- and high latitudes, while the observed time series have broad spring-summer maxima and winter minima.

Disagreement 1 appears to have a complex set of causes: the model's lack of chemistry in the lower stratosphere which counters the model's deficiency in poleward-downward transport; too weak planetary wave driven north-south transport at high latitudes in the troposphere; and finally, the lack of tropospheric chemistry. It is clear that deficiencies in model transport play a major role, though chemistry may also be important.

Separate calculations of the range of chemical tendencies expected at 500 mbar strongly suggest that the lack of a summer maximum in the transport model is due to the missing tropospheric chemistry, though at high latitudes this must be coupled with a summertime minimum at the surface. However, transport control of the ozone precursors must play an important role in the realistic simulation of this highly variable feature. Furthermore, the observed winter minima does not appear to be the result of tropospheric chemistry, which is quite weak or nonexistent at that season. A transport defect in the model, particularly at high latitudes, is the probable explanation.

In order to resolve the role of transport and chemistry in determining the climatology of tropospheric O_3 , the joint measurements of O_3 , NO_x , H_2O , and temperature profiles are needed at a few representative locations for a long enough time to determine accurate climatologies. We are planning to add O_3 , NO_x , and H_2O chemistry to our general circulation transport model and to include a seasonal parameterization in W_0 over land. Furthermore, general circulation transport models with improved cross-tropopause transport, a more realistic boundary layer mixing, and a more active N-S transport at high latitudes are being developed.

Acknowledgments. The authors wish to acknowledge the many helpful comments of S. Manabe, F. C. Fehsenfeld, I. Galbally and M. Prather; the manuscript typing of J. Kennedy, the drafting of P. G. Tunison, W. Ellis, C. Raphael, and M. Zadworney; and the photography of J. Conner. We wish to thank J. London, J. Logan, R. Chatfield, S. Oltmans, and I. Galbally for providing analyzed ozone-sonde and surface time series data before publication. A further special thanks to J. Logan, J. Fishman, and R. Chatfield for many stimulating discussions regarding this work.

REFERENCES

- Aldaz, L., Flux measurements of atmospheric ozone over land and water, *J. Geophys. Res.*, **74**, 6943–6946, 1969.
- Attmannspacher, W., and H. U. Dütsch, 2nd international ozone-sonde intercomparison at the Observatory Hohenpeissenberg, 5–20 April 1978, *Ber. Dtsch. Wetterdienstes* **157**, 1981.
- Attmannspacher, W., and R. Hartmannsgruber, Some results of 6 years (1967–72) of regular ozone soundings at the Meteorological Observatory Hohenpeissenberg, FRG, *Contrib. Atmos. Phys.*, **49**, 18–33, 1976.
- Bojkov, R., Tropospheric ozone, its changes and possible radiative effects, *WMO Spec. Environ. Rep.* **16**, World Meteorol. Organ., Geneva, 1984.
- Chameides, W., and J. C. G. Walker, A photochemical theory of tropospheric ozone, *J. Geophys. Res.*, **78**, 8751–8760, 1973.
- Chatfield, R., and H. Harrison, Tropospheric ozone, 2, Variations along a meridional band, *J. Geophys. Res.*, **82**, 5969–5976, 1977.
- Crutzen, P. J., A discussion of the chemistry of some minor constituents in the stratosphere and troposphere, *Pure Appl. Geophys.*, **106–108**, 1385–1399, 1973.
- Crutzen, P. J., Photochemical reaction initiated by and influencing ozone in unpolluted tropospheric air, *Tellus*, **26**, 58–70, 1974.
- Danielsen, E. F., Stratospheric-tropospheric exchange based on radioactivity, ozone, and potential vorticity, *J. Atmos. Sci.*, **25**, 502–518, 1968.
- Danielsen, E. F., Stratospheric source for unexpectedly large values of ozone measured over the Pacific Ocean during GAMETAG, August 1977, *J. Geophys. Res.*, **85**, 401–412, 1980.
- Danielsen, E. F., and V. A. Mohnen, Project Dustorm report: Ozone transport, in situ measurements, and meteorological analyses of tropopause folding, *J. Geophys. Res.*, **82**, 5867–5877, 1977.
- Dutkiewicz, V. A., and L. Husain, Determination of stratospheric ozone at ground level using ⁷Be/ozone ratios, *Geophys. Res. Lett.*, **6**, 171–174, 1979.
- Dütsch, H. W., Vertical ozone distribution on a global scale, *Pure Appl. Geophys.*, **112**, 915–929, 1974.
- Dütsch, H. W., and C. Ling, Six years of regular ozone soundings over Switzerland, *Pure Appl. Geophys.*, **106–108**, 1139–1150, 1973.
- Fabian, P., A theoretical investigation of tropospheric ozone and stratospheric-tropospheric exchange processes, *Pure Appl. Geophys.*, **106–108**, 1045–1057, 1973.
- Fabian, P., and C. E. Junge, Global rate of ozone destruction at the earth's surface, *Arch. Meteorol. Geophys. Bioklimatol., Ser. A*, **29**, 161–172, 1970.
- Fabian, P., and P. G. Pruchniewicz, Meridional distribution of ozone in the troposphere and its seasonal variations, *J. Geophys. Res.*, **82**, 2063–2073, 1977.
- Fehsenfeld, F. C., M. J. Bollinger, S. C. Liu, D. D. Parrish, M. McFarland, M. Trainer, D. Kley, P. C. Murphy, D. L. Albritton, and D. H. Lenschow, A study of ozone in the Colorado mountains, *J. Atmos. Chem.*, **1**, 87–105, 1983.
- Fishman, J., *O₃ in the Free Troposphere*, edited by R. C. Whitten and S. S. Prasad, Van Nostrand/Rheinhold, New York, 1984.
- Fishman, J., and P. J. Crutzen, A numerical study of tropospheric photochemistry using a one-dimensional model, *J. Geophys. Res.*, **82**, 5897–5906, 1977.
- Fishman, J., and P. J. Crutzen, The origin of ozone in the troposphere, *Nature*, **274**, 855–858, 1978.
- Fishman, J., and W. Seiler, The correlative nature of ozone and carbon monoxide in the troposphere: Implications for the tropospheric ozone budget, *J. Geophys. Res.*, **88**, 3662–3670, 1983.
- Fishman, J., S. Solomon, and P. J. Crutzen, Observational and theoretical evidence in support of a significant in-situ photochemical source of tropospheric ozone, *Tellus*, **31**, 432–446, 1979.
- Galbally, I. E., and C. R. Roy, Destruction of ozone at the earth's surface, *Q. J. R. Meteorol. Soc.*, **106**, 599–620, 1980.
- Gidel, L. T., and M. A. Shapiro, General circulation estimates of the net vertical flux of ozone in the lower stratosphere and the implications for the tropospheric ozone budget, *J. Geophys. Res.*, **85**, 4049–4058, 1980.
- Gregory, G. L., S. M. Beck, and J. A. Williams, Measurements of free tropospheric ozone: An aircraft survey from 46° north to 46° south latitude, *J. Geophys. Res.*, **89**, 9642–9648, 1984.
- Hampson, R. F. (Ed.), Chemical kinetic and photochemical data sheets for atmospheric reactions, *FAA Rep. FAA-EE-80-17*, 490 pp., Fed. Aviat. Agency, Washington, D. C., 1980.
- Hering, W. S., and R. R. Borden, Jr., Ozone-sonde observations over North America, vol. 4, *Rep. AFCRL-64-30(IV)*, Air Force Cambridge Res. Lab., Bedford, Mass., 1967.
- Husain, L., P. E. Coffey, R. E. Meyers and R. T. Cederwall, Ozone transport from stratosphere to troposphere, *Geophys. Res. Lett.*, **4**, 363–365, 1977.
- Junge, C. E., Global ozone budget and exchange between stratosphere and troposphere, *Tellus*, **14**, 363–377, 1962.
- Kirchhoff, V. W. J. H., E. Hilsenrath, A. G. Motta, Y. Sahai, and R. A. Medrano-B, Equatorial ozone characteristics as measured at Natal (5.9°S, 35.2°W), *J. Geophys. Res.*, **88**, 6812–6816, 1983.
- Kley, D., J. W. Drummond, M. McFarland, and S. C. Liu, Tropospheric profiles of NO_x, *J. Geophys. Res.*, **86**, 3153–3161, 1981.
- Lenschow, D. H., A. C. Delany, B. B. Stankov, and D. H. Stedman, Airborne measurements of the vertical flux of ozone in the boundary layer, *Boundary Layer Meteorol.*, **19**, 249–265, 1980.
- Lenschow, D. H., R. Pearson, Jr., and B. B. Stankov, Measurements of ozone vertical flux to ocean and forest, *J. Geophys. Res.*, **87**, 8833–8837, 1982.
- Levy, H., II, Normal atmosphere: Large radical and formaldehyde concentrations predicted, *Science*, **173**, 141–143, 1971.
- Levy, H., II, Photochemistry of the troposphere, *Adv. Photochem.*, **9**, 369–524, 1974.
- Levy, H., II, J. D. Mahlman, and W. J. Moxim, Stratospheric NO_y: A major source of reactive nitrogen in the unpolluted troposphere, *Geophys. Res. Lett.*, **7**, 441–444, 1980.
- Levy, H., II, J. D. Mahlman, and W. J. Moxim, Tropospheric N₂O variability, *J. Geophys. Res.*, **87**, 3061–3080, 1982.
- Liu, S. C., Possible effects on tropospheric O₃ and OH due to NO emissions, *Geophys. Res. Lett.*, **4**, 325–328, 1977.
- Liu, S. C., D. Kley, M. McFarland, J. D. Mahlman, and H. Levy II, On the origin of tropospheric ozone, *J. Geophys. Res.*, **85**, 7546–7552, 1980.
- Liu, S. C., M. McFarland, D. Kley, O. Zafiriou, and B. Huebert, Tropospheric NO_x and O₃ budgets in the equatorial Pacific, *J. Geophys. Res.*, **88**, 1360–1368, 1983.
- Mahlman, J. D., and W. J. Moxim, Tracer simulation using a global general circulation model: Results from a mid-latitude instantaneous source experiment, *J. Atmos. Sci.*, **35**, 1340–1374, 1978.
- Mahlman, J. D., H. Levy II, and W. J. Moxim, Three-dimensional tracer structure and behavior as simulated in two ozone precursor experiments, *J. Atmos. Sci.*, **37**, 655–685, 1980.
- Manabe, S., and J. D. Mahlman, Simulation of seasonal and inter-hemispheric variations in the stratospheric circulation, *J. Atmos. Sci.*, **33**, 2185–2217, 1976.
- Manabe, S., D. G. Hahn, and J. L. Holloway, Jr., The seasonal variation of the tropical circulation as simulated by a global model of the atmosphere, *J. Atmos. Sci.*, **31**, 43–83, 1974.
- McFarland, M., D. Kley, J. W. Drummond, A. L. Schmeltekopf, and R. H. Winkler, Nitric oxide measurements in the equatorial Pacific region, *Geophys. Res. Lett.*, **6**, 605–608, 1979.
- Oltmans, S. J., Surface ozone measurements in clean air, *J. Geophys. Res.*, **86**, 1174–1180, 1981.
- Oltmans, S. J., and W. D. Komhyr, Surface ozone in Antarctica, *J. Geophys. Res.*, **81**, 5359–5364, 1976.
- Parrish, D. D., P. C. Murphy, D. L. Albritton, and F. C. Fehsenfeld, The measurement of the photodissociation rate of NO₂ in the atmosphere, *Atmos. Environ.*, **17**, 1365–1379, 1983.
- Pearson, R., Jr., and D. H. Stedman, Instrumentation for fast response ozone measurements from aircraft, *Atmos. Technol.*, **12**, 51–55, 1980.
- Pittock, A. B., Climatology of the vertical distribution of ozone over Aspendale (38°S, 145°E), *Q. J. R. Meteorol. Soc.*, **103**, 575–584, 1977.
- Routhier, F., R. Dennett, D. D. Davis, A. Wartburg, P. Haagenson, and A. C. Delany, Free tropospheric and boundary layer airborne measurements of ozone over the latitude range of 58°S to 70°N, *J. Geophys. Res.*, **85**, 7307–7321, 1980.
- Seiler, W., and J. Fishman, The distribution of carbon monoxide and ozone in the free troposphere, *J. Geophys. Res.*, **85**, 7255–7265, 1981.
- Singh, H. B., F. L. Ludwig, and W. B. Johnson, Tropospheric ozone: Concentrations and variabilities in clean remote atmospheres, *Atmos. Environ.*, **12**, 2185–2196, 1978.
- Staley, D. O., Strontium-90 in surface air and the stratosphere: Some interpretations of the 1963–75 data, *J. Atmos. Sci.*, **39**, 1571–1590, 1982.
- Stewart, R. W., S. Hameed, and J. P. Pinto, Photochemistry of tropospheric ozone, *J. Geophys. Res.*, **82**, 3134–3140, 1977.

Wesely, M. L., D. R. Cook, and R. M. Williams, Field measurement of small ozone fluxes to snow, wet bare soil, and lake water, *Boundary Layer Meteorol.*, 20, 459-471, 1981.

Wilcox, R. W., and A. D. Belmont, Ozone concentration by latitude, altitude, and month, near 80°W, *Rep. FAA-AEQ-77-13*, U.S. Dep. of Transp., Washington, D. C., 1977.

World Meteorological Organization/NASA, *The stratosphere 1981: theory and measurements*, Geneva, Switzerland, 1981.

H. Levy II, J. D. Mahlman, and W. J. Moxim, *Geophysical Fluid*

Dynamics Laboratory, NOAA, Princeton University, P.O. Box 308, Princeton, NJ 08542.

S. C. Liu, *Aeronomy Laboratory, NOAA, 325 Broadway, Boulder, CO 80303.*

(Received May 14, 1984;
revised November 15, 1984;
accepted November 26, 1984.)